Biological attenuation of arsenic and iron in a continuous flow bioreactor treating Acid Mine Drainage (AMD)

Fernandez-Rojo L.[1], Héry M.[1], Le Pape P.[2], Braungardt C.[3,1], Desoeuvre A.[1], Torres E.[1], Tardy V.[1], Resongles E.[1], Laroche E.[1], Delpoux S.[1], Joulian C.[4], Battaglia-Brunet F.[4], Boisson J.[5], Grapin G.[6], Morin G.[2], Casiot C.[1]

[1] *Hydrosciences Montpellier, UMR 5569 CNRS-IRD-UM, CC57, 163 rue Auguste Broussonet, 34090, Montpellier, France*

[2] *Institut de Minéralogie, de Physique des Matériaux et de Cosmochimie (IMPMC), UMR 7590 CNRS-UPMC-IRD-MNHN, 4 place Jussieu, 75252 Paris cedex 05, France*

[3] *School of Geography, Earth and Environmental Sciences (Faculty of Science & Engineering), Plymouth University, United Kingdom*

[4] *French Geological survey (BRGM), 3 avenue Claude Guillemin, 45060, BP 36009, Orléans Cedex, France*

[5] *IRH Ingénieur Conseil, 197 avenue de Fronton, 31200, Toulouse, France*

[6] *IRH Ingénieur Conseil, 427 rue Lavoisier - CS 50155, 54714, Ludres Cedex, France*

Abstract

Passive water treatments based on biological attenuation can be effective for arsenic-rich Acid Mine Drainage (AMD). However, the key factors driving the biological processes involved in this attenuation are not well-known. Here, the efficiency of arsenic (As) removal was investigated in a bench-scale continuous flow channel bioreactor treating As-rich AMD (~30-40 mg L^{-1}). In this bioreactor, As removal proceeds *via* the formation of biogenic precipitates consisting of iron- and arsenic- rich mineral phases encrusting a microbial biofilm. Fe(II) oxidation and Fe and As removal rates were monitored at two different water heights (4 and 25 mm) and with/without forced aeration. An eighty percent As removal was achieved within 500 min at the lowest water height. This operating condition promoted intense Fe(II) microbial oxidation and subsequent precipitation of As-bearing schwertmannite and amorphous ferric arsenate. Higher water height slowed down Fe(II) oxidation, Fe precipitation and As removal, in relation with limited oxygen transfer through the water column. The lower oxygen transfer at higher water height could be partly counteracted by aeration. The presence of an iridescent floating film that developed at the water surface was found to limit oxygen transfer to the water column and delayed Fe(II) oxidation, but did not affect As removal. The bacterial community structure in the biogenic precipitates in the bottom of the bioreactor differed from that of the inlet water and was influenced to some extent by water height and aeration. Although potential for microbial mediated As oxidation was revealed by the detection of *aioA* genes, removal of Fe and As was mainly attributable to microbial Fe oxidation activity. Increasing the proportion of dissolved As(V) in the inlet water improved As removal and favoured the formation of amorphous ferric arsenate over As-sorbed schwertmannite. This study proved the ability of this bioreactor-system to treat extreme As concentrations and may serve in the design of future *in-situ* bioremediation system able to treat As-rich AMD.

Keywords: arsenic precipitation, bioremediation, iron oxidation, water treatment, biogenic precipitate, ferric arsenate, *aioA* genes, schwertmannite

1. Introduction

Arsenic is ubiquitous in acid mine drainage (AMD) (Williams, 2001; Paikaray, 2015) and represents a severe threat for freshwater resources downstream from mining sites. It is therefore essential to develop treatment processes able to remove arsenic from mine waters. In this respect, co-precipitation with iron is a well-established method (Carlson et al., 2002; Kim et al., 2003; Asta et al., 2010a). When enough iron is originally present in the AMD, addition of a neutralizing agent, such as lime, allows rapid Fe(II) oxidation and subsequent precipitation of simple ferric arsenate ($FeAsO_4$) and ferric hydroxide ($Fe(OH)_3$), or basic ferric arsenate ($FeAsO_4 \cdot xFe(OH)_3$), depending on As/Fe molar ratios (Lawrence and Higgs, 1999). At acid pH, As(III) is poorly retained on Fe-solids. Chemical or photochemical oxidation of As(III) into As(V) might increase As removal efficiency (Emett and Khoe, 2001; Hug and Leupin, 2003).

Alternatively, biological oxidation of iron and arsenic occurs naturally in AMD and has been observed at various mining sites worldwide (Casiot et al., 2003; Asta et al., 2010b; Egal et al., 2010; Chen and Jiang, 2012; Paikaray, 2015). Bacteria involved in iron and arsenic oxidation have been isolated and their metabolic capacities investigated (Battaglia-Brunet et al. 2002, Bruneel et al., 2003). Treatments based on these natural biological oxidation processes are promising because they offer an alternative to active chemical oxidation that is costly and requires periodic maintenance. However, there have been only few attempts to exploit these biological processes for the treatment of As-rich AMD (Battaglia-Brunet et al., 2006; Elbaz-Poulichet et al., 2006; Macías et al., 2012; Ahoranta et al., 2016) and the factors controlling the efficiency of this natural process, ranging from 7% to nearly 100% As removal, are still poorly understood. Lessons learnt from AMD observations drew attention to the remarkable efficiency of terraces and waterfalls, as compared to pools, for arsenic retention (Asta et al., 2010b; Chen and Jiang, 2012; Macías et al., 2012). Chen and Jiang (2012) hypothesized that

turbulent flow conditions and shallow water in waterfall sections maximized the iron oxidation rate by improving oxygen diffusion. In this respect, Brown et al. (2011) also found in laboratory experiments that greater Fe(II) oxidation occurred at lower water height. Conversely, quiescent pools, by favouring the development of an iridescent oil-like floating film at the water surface (Kleja et al., 2012), were suspected to limit the efficiency of the treatment (Elbaz-Poulichet et al., 2006).

In the present study, a bench-scale continuous flow bioreactor was used to identify the major factors controlling the efficiency of microbially-mediated arsenic removal from AMD. The system was supplied with AMD from the Carnoulès mine (Southern France), where extreme arsenic concentrations and natural arsenic attenuation involving biological Fe and As oxidation had been evidenced (Leblanc et al., 1996; Bruneel et al., 2003; Casiot et al., 2003; Morin et al., 2003; Egal et al., 2010). The microbial, chemical and mineralogical composition of the biogenic precipitate naturally developing on the bottom of the channels was also investigated. The As molecular level speciation and redox state in the solid and aqueous phases was investigated using X-ray absorption spectroscopy and high performance liquid chromatography-inductively coupled plasma-mass spectrometry (HPLC-ICP-MS), respectively. The results yield evidence for the effect of water height and floating film on the rate of microbial Fe(II) oxidation and Fe and As precipitation at acid pH.

2. Materials and methods

2.1 Continuous flow bioreactor design

Experiments were conducted in a bench-scale bioreactor (Fig. 1A), reproducing the shallow sheet flow commonly seen across natural terraced iron formations (TIFs) described in AMD (Sánchez-España et al., 2007; DeSa et al., 2010; Brown et al., 2011; Larson et al., 2014). It

was composed of four rectangular polyvinyl chloride channels (1 m length × 0.06 m width × 0.06 m depth), each equipped with a double envelope for temperature control. A biodegradable canvas of polylactic acid (BIO DURACOVER) was placed on the bottom of each channel to provide a rough surface for the adhesion of the biogenic precipitate. Preliminary tests showed that the mineralogy, concentrations of As and Fe, and microbiology (number of bacterial cells and bacterial community structure) in the precipitate formed on this material were similar to the one formed on an inert plastic net (Direct-Filet.com, mesh size of 1.4 mm × 0.83 mm). Thus, the cost-effective biodegradable canvas was chosen.

A four-channel peristaltic pump (Gilson, Minipuls 3) simultaneously supplied the four channel inlets with AMD at specific flow rates that determined the water residence time (~ 20-1800 min). A second peristaltic pump was used to remove the fluid from the experimental set-up through holes drilled in the terminal sections of the channels, and to maintain the water level at specific heights. C-Flex® tubing (i.d. 3.2 mm), was joined by polypropylene connectors (i.d. 3.1 mm) to peristaltic pump tubing (Tygon® i.d. 3.17 mm) and to the channel inlets and outlets. A 3-way valve was positioned at the end of each outlet tube for sample collection. Treated effluent from the experiments was collected and periodically returned to the mining site. The temperature in the double envelope of the channels was maintained at 20 ± 0.8 °C by continuous circulation of a cooler-heating fluid (Julabo Thermal G) in a closed circuit, connected to a temperature control unit (Julabo F34-EH). Air conditioning was settled to 20 °C in the laboratory. The channels were illuminated with a neon lamp (T5 Superplant 216W CROISSANCE 6500 K) in the 400-500 nm spectra, with a photon flux density of 0.8 µmol m^{-2} s^{-1}, and a day/night cycle of 12 h.

2.2 AMD feed water sampling and preservation

AMD was collected on the 20th January, 12th February, and 23rd March 2015, from the spring of Carnoulès Creek. Containers (20 L, high density polyethylene) were decontaminated with

concentrated HNO_3, rinsed three times with double deionized water (DDW, Milli-Q®) and finally with *in-situ* AMD before sample collection. The filled containers were immediately transported to the laboratory and then purged with N_2 until DO decreased below 1 mg L^{-1}, in order to avoid iron oxidation. Containers were stored at 20 °C in the laboratory and used in turn under N_2 purge during the course of the experiment to supply water to the bioreactor. The main physico-chemical parameters, Fe and As dissolved concentrations (total and individual species) were checked at the opening of each new container.

2.3 Flow bioreactor experiments

Two experiments referred to as Exp 1 and Exp 2 were conducted in the bioreactor. During the setting up stage of the experiments, lasting 10-15 days, the water height was maintained at 4 mm and the flow rate was fixed at 0.5 mL min^{-1}, equivalent to a residence time (RT) of 324 ± 30 min. Inlet and outlet water was collected at regular time intervals for dissolved Fe(II) and total dissolved Fe determination until steady-state was reached with respect to Fe(II) oxidation (Fig. 2). After this timeframe, kinetic studies were carried out for Fe(II) oxidation, total Fe precipitation, and As(III), As(V), and total As removal (Fig. 3). For that purpose, the flow rate was set to successively achieve specific residence times: ~ 20 min, ~50 min,… ~1800 min. The exact residence times were calculated as described in paragraph 2.4.2. After each change in flow rate, the system was allowed to adjust for a minimum of three residence times before inlet and outlet water chemistry (Fe(II), total Fe, As(III), As(V) and total As in the dissolved phase) were determined, using routine sampling and preservation procedures described in section 2.4.1 and in the Supporting Information file (SI-Experimental part).

In both Exp 1 and Exp 2, a thin iridescent, oil-like film, referred as “pellicle biofilm” or “floating film” in the literature, spontaneously formed on the water surface.

Exp 1 was conducted at 4 mm water height and investigated the effect of the floating film. Accordingly, the kinetic study Exp $1_{(FF)}$ was first conducted in presence of a floating film

149 (FF), on four replicate channels. Six days after the beginning of the kinetic study, the
150 experiment was stopped in two of the channels and the biogenic precipitate was recovered for
151 analysis. In the two other channels the floating film was removed with a spatula and a kinetic
152 study was carried out in open air (OA) for 17 days more (Exp 1 $_{(OA)}$).
153 Exp 2 was conducted at two water heights in parallel, 4 mm (Exp 2 $_{(4\ mm)}$) and 25 mm (Exp
154 2 $_{(25\ mm)}$), with two replicate channels each. To prevent the formation of the floating film, the
155 water surface was agitated daily with a spatula. A thin plastic film (HP transparency film, 60
156 mm x 60 mm) was positioned vertically in the channels parallel to the flow direction, in order
157 to sample the biogenic precipitate accumulated along a vertical profile during the experiment.
158 After 8 days of kinetic study, one of the 25 mm-water-height channels was aerated using an
159 aquarium pump and ceramic air diffusers (Hagen, Marina A983), positioned at 3 cm and 50
160 cm from the inlet, and another kinetic study (Exp 2 $_{(25\ mm,\ Air)}$) was performed.

161 ### *2.4 Experiment monitoring*

162 #### *2.4.1 Water chemistry analysis*

163 Water chemistry analyses included measurement of the DO, temperature, pH, conductivity
164 and redox potential as well as the determination of concentrations of dissolved Fe(II) and
165 sulphate using spectrophotometry, and total dissolved Fe and As using ICP-MS, after 0.2 µm
166 filtration. Arsenic redox speciation was determined using HPLC-ICP-MS. Dissolved oxygen
167 depth profiles in the water column of bioreactor channels were acquired using
168 microelectrodes. Details of these analytical procedures are reported in SI-Experimental part.

169 #### *2.4.2 Calculation of residence times and reaction rates*

170 The RT, in seconds, was determined for each flow rate value dividing the empirical volume of
171 water (in mL) recovered from the channel, by the flow rate (in mL s^{-1}) measured at the

channel inlet. Fe(II) oxidation, Fe- and As-removal rates (in mol L^{-1} s^{-1}) were calculated using Eq. (1);

$$\text{Rate} = \frac{([X]inlet - [X]outlet)}{RT} \quad (1)$$

where [X] was the dissolved concentration of Fe(II), total Fe, total As, As(III) or As(V), respectively, in mol L^{-1}. It was not possible to calculate with the Eq. (1) the As(III) oxidation rate for a specific residence time, because dissolved As(III) may be removed from solution by precipitation of As(III)-Fe(III) minerals, oxidation to As(V) and/or precipitation of As(V)-Fe(III) minerals. Thus, only As(III) and As(V) removal rates were determined.

2.4.3 Water microbial analysis

At the beginning of the experiments, subsamples of bioreactor feed water were collected for microbiological characterization. Triplicates of 1 mL subsamples were analysed by flow cytometry for bacterial quantification. In addition, triplicates of 300 mL-subsamples were filtered (pore size 0.2 µm, cellulose acetate), and the filter membranes stored at -80 °C for further DNA extraction and bacteria community analysis by automated ribosomal intergenic spacer analysis (ARISA) fingerprints (see SI-Experimental part for details).

2.4.4 Biogenic precipitate characterization

The biogenic precipitates from Exp 1 $_{(FF)}$, Exp 1 $_{(OA)}$, Exp 2 $_{(4\ mm)}$, Exp 2 $_{(25\ mm)}$ and Exp 2 $_{(25\ mm,\ Air)}$ were recovered from the bottom of the channels at the end of each experiment and characterized for their mineralogy, As and Fe content, As speciation, bacterial cell number, bacterial genetic fingerprint, and *aioA* genes quantification. For this purpose, water was removed from each experimental channel and collected in a graduated cylinder to determine water volume. The biogenic precipitate that formed at the bottom of the channel was recovered by scraping the biodegradable canvas with a sterilized spatula and transferred to Eppendorf tubes (2 mL). Three aliquots were used as replicates for the bacterial

quantification, one aliquot was used for DNA extraction, ARISA, rRNA 16S and *aioA* genes quantification (SI-Experimental part), one for total Fe and As determination after acid digestion, and the last aliquot for mineralogy, including X-ray diffraction (XRD), X-ray absorption near edge structure (XANES) at the As K-edge, and extended X-ray absorption fine structure (EXAFS) at both the As and Fe K-edges (see SI-Experimental part for details).

Typical floating films were sampled at the water surface in the bioreactor, dried in a desiccator under vacuum atmosphere, coated with Pt (SC7620 Quorum technologies) and examined with a scanning electron microscope (SEM; Hitachi S4800). The floating film from the Exp 1 $_{(FF)}$ was analysed by EXAFS at the As and Fe K-edges.

The vertical plastic films inserted in Exp 2 were transferred into a plastic box and dried in N_2 atmosphere with minimum disturbance for direct spatially resolved XANES and micro-X-ray fluorescence measurements and for electron microscopy analyses using a SEM-FEG Zeiss® Ultra55 microscope (see SI-Experimental part for details).

3. Results

3.1 Chemistry of inlet AMD water

Chemical composition of the AMD feed waters (Table 1) exhibited natural variability in the Carnoulès mine drainage (Casiot et al., 2003; Egal et al; 2010). The mean values for pH (3.0-3.4), conductivity (2.87-3.21 mS cm^{-1}), total dissolved Fe concentration (441-484 mg L^{-1}), dissolved Fe(II) (432-480 mg L^{-1}) and total dissolved As (mean 30-39 mg L^{-1}) varied only slightly among the AMD sampling campaigns. In contrast, oxidation state of dissolved arsenic varied among the sampling campaigns and evolved over time (mean 16-57 % As(V)/total As).

3.2 Setting up the steady-state in the continuous flow bioreactor

During the setting up stage of the experiments, the outlet Fe(II) concentration decreased as a function of time, while the Fe(II) concentration in the feed water remained nearly constant (Fig. 2). Concomitantly, the amount of Fe precipitated increased (Fig.2) and a thin orange deposit gradually covered the bottom of the channels (Fig. 1B). After ~ 10 days (Exp 1) and ~ 15 days (Exp 2), the Fe(II) concentration at the outlet remained stable, showing that steady-state conditions were reached regarding Fe(II) oxidation. Under steady-state, the dissolved Fe(II) concentration in the outlet was higher in Exp 2 (~250 mg L^{-1}) than in Exp 1 (~ 50 mg L^{-1}).

3.3 Variation of the amount of oxidized Fe(II) and precipitated Fe and As in kinetic studies

Increase in residence time was found to systematically improve Fe oxidation, Fe precipitation and As removal, however, there were substantial differences between experiments. Exp 1 $_{(OA)}$ showed the highest rate of Fe oxidation and precipitation (Fig. 3AB, Table 2). In Exp 1 $_{(FF)}$, delayed Fe(II) exhaustion and Fe removal were observed for residence times below 150 minutes (Fig. 3A). Exp 2 $_{(4\ mm)}$ exhibited lower rates of Fe(II) oxidation and Fe and As removal than Exp 1 $_{(OA)}$ (Fig. 3ABC, Table 2). Finally, in Exp 2 $_{(25\ mm)}$, Fe(II) oxidation, Fe precipitation and As removal were drastically slower than in the other experiments (Fig. 3ABC, Table 2); only the highest residence times (> 1000 min) showed significant Fe(II)-, Fe-, and As-exhaustion and pH decrease. After forced aeration in Exp 2 $_{(25\ mm,\ Air)}$, the average rates of Fe(II) oxidation and Fe removal increased approximately two-fold, while the As removal rate increased no more than 1.6-fold (Fig. SI-1). As(V) removal was systematically more efficient than As(III) removal in all experiments (Fig. 3DE). Consequently, dissolved arsenic in the outlet consisted mainly of As(III) (Fig. 3CD).

3.4 Oxygen concentration profiles

The DO profile recorded in the water column at 4 mm water height in absence of a biogenic precipitate at the bottom of the channels (Fig. 4A) showed oxygen saturation concentrations in the whole water column. On the contrary, after biogenic precipitate had formed (profiles from Exp $1_{(OA)}$ and Exp $2_{(4\ mm)}$), oxygen was consumed in the water column. The DO profiles showed saturation at the water surface and gradual concentration decrease from 8.7 to 5.7 mg L^{-1} within the first 1 mm depth, then a further decrease to ~ 2.0 mg L^{-1} at the interface between the water column and the biogenic precipitate. The floating film limited oxygen concentration to less than 0.01 mg L^{-1} for depths below 1 mm.

The DO profile at 25 mm water height showed a rapid decrease from saturation value (8.0 mg L^{-1}) at the water surface to less than 4.0 mg L^{-1} below 20 mm, then relatively constant value at 3.9 ± 0.3 mg L^{-1} near the biogenic precipitate. After aeration in Exp $2_{(25\ mm,\ Air)}$, the DO concentration in the water column averaged 6 ± 1 mg L^{-1}, according to three measurements carried out at inlet, middle and outlet of the channel (micro-profiling was not possible due to turbulent conditions).

3.5 Arsenic speciation and mineralogy in the biogenic precipitates and floating film

The biogenic precipitates at the channel bottom contained ~35 wt. % Fe and ~7 wt. % As, with an As/Fe molar ratio ranging from 0.14 to 0.20 (Table 3). XRD analysis (Table 3, Fig. SI-2), showed that the nano-crystalline fraction of the solid phase was similar irrespective of the experiment conditions, consisting mainly of schwertmannite. Fe K-edge EXAFS data (Fig. 5, Table 3, Table SI-3 and Fig. SI-4) revealed the additional presence of 15-33 mol% amorphous ferric arsenate, in mixture with 67-85 mol% of schwertmannite. K-edge XANES indicated 16-52 % As(III)/Total As and 48-84 % As(V)/Total As in the biogenic precipitates (Table 3, data from Resongles et al. (2016), see Table SI-1 for equivalence of sample names).

K-edge EXAFS (Fig. 5, Table 3, Table SI-2 and Fig. SI-3) showed that As(III) and As(V) species were distributed among three different solid phases: schwertmannite with As(III) (16 to 51 mol%), schwertmannite with As(V) (20 to 38 mol%) and amorphous ferric arsenate (31 to 62 mol%). The floating-film collected in Exp $1_{(FF)}$ had similar composition as the precipitates collected at the bottom of the reactor in the same experiment (Table 3). SEM images showed that the nature of this floating film consisted of a mineralogical layer with numerous bacteria, some of which were encrusted by mineral precipitates (Fig SI-6A) with similar morphology as those observed on the vertical plastic film and at the bottom of the bioreactor channels (Fig SI-6BC).

The arsenic oxidation state in the biogenic precipitates varied significantly among the experiments. Indeed, the proportion of As(V) was higher in Exp 1 than in Exp 2 (Fig. 5, Table 3). In addition, increasing the water height in Exp 2 resulted in a higher proportion of As(V), mainly in the form of amorphous ferric arsenate in the precipitate (Fig. 5). The effect of the water height was confirmed by spatially resolved XANES and micro-X-ray fluorescence analyses of the precipitates deposited on the vertical plastic film in Exp 2 (Fig. 6 and Fig. SI-7). In Exp $2_{(4\ mm)}$, the proportion of As(V) in the precipitate remained below 50% and decreased from ~50% at the bottom of the channel to ~ 30% at the water surface (Fig. 6A). In Exp $2_{(25\ mm)}$, similar behaviour was observed up to 5 mm water height and the proportion of As(V) then largely increased, up to ~ 60-80%, at the top of the water column. Air bubbling in Exp $2_{(25\ mm\ Air)}$ slightly decreased the proportion of As(V) in the precipitates that formed in the water column. These variations of the proportion of As(V) were positively correlated to the As/Fe molar ratio in the precipitates (Fig. 6B).

3.6 Microbial characterization of the biogenic precipitates

289 Bacterial biomass within the bottom biogenic precipitates remained in the same order of
290 magnitude between the experiments, with an average of $6 \pm 4 \times 10^6$ bacterial cells g^{-1} (dry
291 weight) (Table 3).

292 The bacterial community in the biogenic precipitates differed widely from that in the
293 corresponding feed waters (Fig. 7). Concerning the different experimental conditions, the
294 structure of the community does not seem to have been affected notably by the presence of
295 the floating film (Exp 1 $_{(FF)}$ and Exp 1 $_{(OA)}$). Conversely, water height appeared as a potential
296 factor influencing the bacterial community structure; indeed, the bacterial community from
297 Exp 2 $_{(25\ mm)}$ is well discriminated from all the communities obtained at 4 mm water height
298 and from the community exposed to air bubbling (Exp 2 $_{(25\ mm,\ Air)}$). The variation in the
299 bacterial community of the biogenic precipitates of the similar experiments Exp 1 $_{(OA)}$ and
300 Exp 2 $_{(4\ mm)}$ can be linked at least partially to the different feed waters. *aioA* genes were
301 detected in the biogenic precipitates in all experiments. The proportion of bacteria possessing
302 the genetic potential for As(III) oxidation averaged 25 % of the total community (mean
303 *aioA*/16S ratio of 0.25, Table 3) .

304

305 **4. Discussion**

306 ***4.1 Fe(II) oxidation and precipitation in the channel bioreactor: influence of the***
307 ***microbial community***

308 The channel bioreactor allowed to achieve Fe(II) oxidation and subsequent Fe precipitation,
309 providing the basis for arsenic removal. In the setting up stage of the continuous flow
310 experiments (Fig. 2), the gradual increase of the Fe(II) oxidation rate was concomitant to the
311 microbial colonization of the bottom of the bioreactor channels. This highlighted the role of
312 microorganisms developing within the biogenic precipitate as catalysts for Fe(II) oxidation.

313 The biogenic precipitates contained 3-9 $\times 10^6$ bacterial cells g^{-1} dry wt., which was
314 comparable to the Carnoulès sediment content (3×10^6 cells g^{-1} dry wt., Desoeuvre, personal
315 communication) and to other TIFs, for which generally 10^6-10^7 bacterial cells g^{-1} have been
316 reported (Brown et al., 2011; Brantner et al., 2014).

317 Bacteria colonizing the biogenic precipitate in the channel bioreactor were inherited from the
318 seed community present in AMD water from the Carnoulès mine. Fe(II)-oxidizing bacteria
319 are likely to belong to the genera *Gallionella* and *Acidithiobacillus*, which are known to be
320 permanent members of the Carnoulès AMD autochthonous community (Volant et al., 2014).
321 In spite of the wide variability of the water bacterial community structure, relatively similar
322 communities were selected within the biogenic precipitates originating from different waters
323 (Fig. 7); these biogenic precipitates allowed to maintain over 50 % Fe(II) oxidation within a
324 residence time of 300 min, in all the experiments conducted at 4 mm water height. This
325 corroborated the findings of Sheng et al. (2016) who obtained efficient Fe(II) oxidizing
326 activity with different seed AMD communities in chemostatic bioreactors treating AMD.

327 The average Fe(II) oxidation rate ($3.4 \pm 0.9 \times 10^{-7}$ mol L^{-1} s^{-1}) ranged within literature values
328 for other natural or engineered TIFs (Larson et al., 2014, and references therein). However,
329 Fe(II) oxidation rates differed slightly between Exp 1 $_{(OA)}$ and Exp 2 $_{(4\ mm)}$ carried out in the
330 same operating conditions (Fig. 3), with similar feed water physico-chemistry in term of pH,
331 Fe(II) and As concentration (Table 1). This suggests that slight variations in the structure or
332 the activity of the bacterial community may affect Fe(II) oxidation rates to some extent.
333 Further insight into the taxonomic composition of the bacterial community would be required
334 to check this hypothesis.

335 ### *4.2 Influence of floating film on Fe(II) oxidation in the channel bioreactor*

336 The floating film formed in these experiments consisted of schwertmannite and amorphous
337 ferric arsenate associated with bacteria. Such mineralogy logically differed from that found in
338 floating films from circum-neutral pH waters where ferrihydrite was dominant (Grathoff et
339 al., 2007; Kleja et al., 2012). The identity of bacteria evidenced in this floating film is still
340 unknown; elsewhere, the sheathed bacterium *Leptothrix* (van Veen et al., 1978; Robbins et al.,
341 2000; Eggerichs et al., 2014) and other genera (Wilmes et al., 2009; Reina et al., 2015) have
342 been identified.

343 To our knowledge, the effect of the floating film on the functioning of natural or engineered
344 TIFs, regarding Fe(II) oxidation, had never been investigated before. In the kinetic study of
345 Exp 1 $_{(FF)}$, delayed Fe(II) exhaustion observed for residence times below 150 minutes, was
346 associated with anoxic conditions in the water column below 1 mm depth (Fig. 4A). Oxygen
347 depletion had been evidenced below floating iron-oxide films that formed at circum-neutral
348 pH in several groundwater seepage areas of the Doñana National Park (SW Spain) compared
349 with other film-free wetland areas (Reina et al., 2015). Puyate and Rim-Rukeh (2008)
350 suggested that in biofilms, bacteria embedded in a slime of extracellular polymeric substances
351 used oxygen as a nutrient and depleted the DO concentration in the surrounding liquid
352 medium. Thus, it was anticipated that faster rates of metabolic consumption, relative to the
353 oxygen diffusion rate, induced a decline in concentrations of DO with increasing distance
354 from the air–solution interface. In batch experiments carried out with AMD from Esperanza
355 mine, the lack of oxygen resulting from standing conditions in a tank induced a slowdown in
356 Fe(II) oxidation compared to aerated conditions, showing that oxygen transfer was a limiting
357 factor (Sánchez-España et al., 2007). More specifically, studies dedicated to the Fe(II)
358 oxidation kinetics by *A. ferrooxidans* have reported that the mesophilic oxidation rate of
359 ferrous iron with air was limited by the oxygen transfer rate (Savić et al., 1998). According to
360 Liu et al. (1988), a DO value below 0.29-0.7 mg L^{-1} was limiting for *A. ferrooxidans*.

361 It can be hypothesized that the floating film, by limiting oxygen transfer rate at the air/water
362 interface, lowered oxygen concentration in the water column, which had an adverse effect on
363 the activity of iron oxidizing populations, such as *A. ferrooxidans*, and this effect was most
364 pronounced at low residence times (< 150 min) in the bioreactor. However, the floating film
365 had a limited influence on the whole bacterial community structure (Fig. 7).

366 ### *4.3 Influence of water height on Fe(II) oxidation in the channel bioreactor*

367 The increase of water height in Exp 2 was associated to several changes that may explain
368 Fe(II) oxidation slowdown: i) the bacterial cell concentration in the biogenic precipitate was
369 slightly lower at 25 mm ($4.4 \pm 0.6 \times 10^6$ cells g^{-1} dry wt.) than at 4 mm ($9 \pm 5 \times 10^6$ cells g^{-1}
370 dry wt.), ii) the bacterial community structure was slightly different (Fig. 7), iii) oxygen
371 concentration was depleted in the water column and iv) the ratio between the volume of water
372 in the channel and the surface of the biogenic precipitate was ~ 6-fold higher in Exp 2 $_{(25mm)}$
373 compared to Exp 2 $_{(4mm)}$.
374 The key role of oxygen transfer was evidenced in Exp 2 $_{(25\ mm,\ Air)}$, considering the 2-fold
375 improvement of the Fe oxidation rate resulting from air bubbling. Turbulent flow conditions
376 favour mass transfer and oxygen diffusion (Eberl et al., 2000; Wäsche et al., 2002; Beyenal
377 and Lewandowski, 2002). Brown et al. (2011) hypothesized an effect of hydrodynamic
378 conditions (e.g., sheet flow and turbulence) on Fe(II) oxidation rates and subsequent treatment
379 system performance in Lower Red Eyes AMD (Pennsylvania). Chen and Jiang (2012)
380 observed that AMD creek sections in Chinkuashih (Taiwan) exhibited Fe(II) oxidation rates
381 that were one to two orders of magnitude slower than in waterfall sections, where Fe
382 oxidation rates reached 6.1 to 6.7×10^{-6} mol L^{-1} s^{-1}. They suggested that waterfall aeration
383 was the main factor driving up the Fe(II) oxidation rate and pointed out the dynamic splashing
384 effects on chemical transport.

385 The reactive surface area per volume of water is also a key parameter driving Fe(II) oxidation
386 rate in fixed-film continuous flow bioreactors. As an example, a ~ 2-fold increase of surface
387 area allowed a ~ 2-fold increase of Fe(II) oxidation rate in a packed bed reactor working with
388 glass beads as a support matrix (Grishin and Tuovinen, 1988). It is therefore anticipated that
389 lower Fe(II) oxidation rate in Exp 2 $_{(25\ mm)}$ is partly related to higher water volume to reactive
390 surface area ratio.

391 ***4.4 Arsenic oxidation and removal in the channel bioreactor***

392 *4.4.1 Arsenic removal*

393 The removal of arsenic concomitantly to Fe, so called "natural attenuation", has been
394 described in several AMD throughout the world (e.g. Cheng et al., 2009; Rait et al., 2010;
395 Paikaray, 2015). In AMD, arsenic is generally removed from the dissolved phase by sorption
396 onto schwertmannite (Carlson et al., 2002; Fukushi et al., 2003; Ohnuki et al., 2004) or
397 formation of amorphous ferric arsenate (Maillot et al., 2013). In addition, a rare ferric arsenite
398 phase (tooeleite) may occasionally occur at high As concentration (Morin et al., 2003). The
399 rate of this removal has rarely been determined either in treatment trials or in natural AMD. In
400 a recent study with a fluidized bed reactor inoculated with an iron-oxidizing culture and added
401 flocculant, Ahoranta et al. (2016) obtained an As removal rate of 1.4-1.7 $\times 10^{-10}$ mol L^{-1} s^{-1},
402 reaching 99.5 % As removal with a retention time of 342 min at pH 3. Asta et al. (2010b)
403 measured an As(V) removal rate of 7-8 $\times 10^{-10}$ mol L^{-1} s^{-1} in the Tinto Santa Rosa AMD.
404 Chen and Jiang (2012) obtained 4.7-6.3 $\times 10^{-9}$ mol L^{-1} s^{-1} for the As sorption rate in AMD
405 waterfall section from the Chinkuashih area.

406 In the present study, arsenic was efficiently removed from the dissolved phase in the channel
407 bioreactor when it operated at 4 mm in open air, reaching 65 % abatement within 500 minutes
408 (Fig. 3). This corresponded to an average removal rate of ~ 4 $\times 10^{-8}$ mol L^{-1} s^{-1}, one order of
409 magnitude lower than in the field at Carnoulès (3.58 $\times 10^{-7}$ mol L^{-1} s^{-1}; Egal et al., 2010).

The faster As removal in the field may be associated with faster Fe(II) oxidation rates (3.8×10^{-6} mol L^{-1} s^{-1}) and subsequent precipitation, compared to the laboratory (Fe oxidation rate = $3.4 \pm 0.9 \times 10^{-7}$ mol L^{-1} s^{-1}), which was also observed in other studies (Sánchez-España et al., 2007; Larson et al, 2014). Photochemical As(III) oxidation in addition to microbial As(III) oxidation, may also favour As removal (Asta et al., 2012), since As(V) is less soluble than As(III) at acidic pH (Burton et al., 2009).

The arsenic removal rate was ten-fold lower in Exp 2 $_{(25\ mm)}$, compared to Exp 2 $_{(4\ mm)}$ (Table 2). The higher outlet pH in Exp 2 $_{(25\ mm)}$, compared to other experiments (Fig. 3F) should have favoured the sorption of As(III) on schwertmannite (Burton et al;, 2009); however, it was limited by the lower amount of Fe(II) oxidized. Conversely, the higher pH was not expected to significantly affect As(V) sorption on schwertmannite, which is more readily sorbed than As(III) within this acid pH range (Burton et al., 2009). Similarly, there was no clear evidence for a retardation of the As removal by the floating film, in relation with the higher proportion of more readily precipitated As(V) in the feed water in Exp 1 $_{(FF)}$ (57 %) compared to Exp 1 $_{(OA)}$ (39 %).

4.4.2 Arsenic oxidation

According to mass balance calculations (SI-Experimental part), the amount of As(V) accumulated in the biogenic precipitate was higher than the amount of As(V) removed from the dissolved phase (Fig. SI-5), showing that arsenic oxidized to some extent in the bioreactor. In addition, the detection of *aioA* genes suggests that microbially mediated arsenic oxidation occurred within the bioreactor, in agreement with the sustained detection of an As-oxidizing activity in the Carnoulès AMD (Casiot et al., 2003), particularly attributable to *Thiomonas* spp. (Bruneel et al., 2003; Hovasse et al., 2016). The relative abundance of *aioA*-carrying bacteria in the biogenic precipitates was higher than in waters moderately contaminated with arsenic (Quéméneur et al., 2010) and in geothermal springs (Jiang et al.,

2014). Nevertheless, the abiotic oxidation of arsenic cannot be totally ruled out; indeed, Fe(III) originating from bacterial Fe(II) oxidation may oxidize As(III) in the presence of visible light (Bhandari et al., 2011; Asta et al., 2012). Furthermore, As(III) oxidation may occur prior to precipitation but also during ageing of the precipitate. In this respect, Ona-Nguema et al. (2010) showed that oxidation of Fe(II) can lead to the formation of reactive oxygen species able to oxidize As(III) to As(V) at the surface of iron oxides or oxyhydroxides at neutral pH, while Burton et al. (2009) indicated that As(III) sorbed on schwertmannite did not undergo abiotic oxidation in oxic conditions, within a period of 2.5 days.

Considering both As(III) concentration remaining in the dissolved phase (Fig. 3D) and the proportion of As(III) (16 – 52 %) in the final precipitate (Table 3), As(III) oxidation was not complete in the present experiments. The data indicates first order kinetics for As(III) exhaustion in Exp 1 $_{(OA)}$ (Fig. 3D), and assuming that all exhausted As(III) has been oxidized, a kinetic constant value k = 0.0065 min^{-1} and half-life value $t_{1/2}$ = 107 min were determined. This is at least one order of magnitude lower than k values obtained in fixed-bed bioreactors working at higher pH, inoculated with the As-oxidizing bacteria *Thiomonas arsenivorans* (k ≈ 0.05 min^{-1}, $t_{1/2}$ = 13.6 min in Wan et al., 2010) or a consortium (k ≈ 0.04 min^{-1}, $t_{1/2}$ = 16.5 min in Michon et al., 2010) originating from a gold mine site, used for the treatment of As(III)-rich groundwater. Thus, although biogenic precipitates formed in the bioreactor contain a substantial proportion (average of 25 %) of As-oxidizing bacteria, the operating conditions tested in this study did not appear to favour their activity. A number of factors may influence their activity. Debiec et al. (2017) showed that pH, temperature and aeration impacted the rate of As(III) oxidation in cultures of As-oxidizing strain *Sinorhizobium* sp. M14, isolated from an arsenic-contaminated mine. In the present study, both a lower water height that favours oxygen diffusion to the biogenic precipitate, and air bubbling, increased the rate of As removal; however it did not increase arsenite oxidizer abundance (*aioA* gene), nor the

proportion of As(V) in the precipitate, which was even lower in Exp 2 $_{(4\ mm)}$ than in Exp 2 $_{(25\ mm)}$. This suggested that oxygen diffusion to this precipitate was not a key factor driving arsenite oxidation and removal from the water, contrary to Fe oxidation. Most probably, the rate of As(III) exhaustion and the proportion of As(III) and As(V) in the biogenic precipitate were controlled by the rate of Fe(II) oxidation and subsequent precipitation, as well as by the As(V) proportion in the inlet water. Higher Fe(II) oxidation and Fe precipitation rates in Exp 2 $_{(4\ mm)}$, compared to Exp 2 $_{(25\ mm)}$, favoured the rapid achievement of the schwertmannite solubility product, and subsequent sorption of As(III) and As(V), before appreciable As(III) oxidation took place. Another hypothesis could be that As-oxidizing bacteria may be more active or more numerous in the water column than Fe-oxidizing bacteria. In this respect, Michel et al. (2007) showed that the specific As(III)-oxidase activity of *Thiomonas arsenivorans* was higher (9-fold) for planktonic cells than for sessile ones. Similarly, in the deposits along the vertical plastic film, the higher proportion of As(V) and higher As/Fe molar ratio (Fig. 6), at greater distance from the biogenic precipitates, suggests the occurrence of vertical gradients of Fe(II) oxidation and As(III) oxidation within the water column. Further research is required to find out key factors able to influence the growth and As-oxidizing activity of microorganisms in the bioreactor. Nevertheless, since As(III) oxidation was limited in the bioreactor, the proportion of As(V) in the inlet water (Table 1) largely influenced the As removal rate, since As(V)-bearing precipitates are ten times less soluble than As(III) ones at acidic pH (Burton et al., 2009; Maillot et al., 2013).

4.4.3 Control of dissolved As(V) and Fe(III) on the mineralogy of the biogenic precipitates

The formation of amorphous ferric arsenate over schwertmannite is favoured by an increase in the As(V)/Fe(III) ratio in solution. Indeed, the high affinity of As(V) oxyanions for the complexation with Fe(III) has been shown to inhibit the nucleation of schwertmannite and to

favour the formation of amorphous ferric arsenate for dissolved As(V)/Fe(III) ratio above 0.15-0.2 (Carlson et al., 2002; Maillot et al., 2013). In the present study, for residence times between ~ 20-500 min, the range of dissolved As(V)/Fe(III) molar ratios removed from the dissolved phase (Fig. 3) increased in the order: Exp 2 $_{(4\ mm)}$ (< 0.01-0.11) < Exp 1 $_{(OA)}$ (< 0.01-0.18) < Exp 2 $_{(25\ mm)}$ (0.09-0.38) < Exp 1 $_{(FF)}$ (0.02-1.68). The proportion of ferric arsenate increased accordingly (Fig. 5), thus corroborating the influence of both dissolved As(V) proportion in the inlet and Fe(II) oxidation rate on the proportion of ferric arsenate in the biogenic precipitate.

5. Conclusions

Within the continuous flow bioreactor designed for this study more than 80 % of Fe(II) was oxidised and ~ 65 % of As was removed from As-rich (30-40 mg L^{-1}) AMD within 500 min. The treatment produced sludge with high As concentration (6.3-8 % dry wt.), mainly in the less toxic As(V) form (49-85 %). Distinct feed waters, in term of chemical and microbiological composition, led to the settlement of relatively constant bacterial community in the bioreactor capable to catalyse the Fe(II) oxidation and the As removal. Such resilience is promising for future *in situ* treatment of AMD.

This study contributes to a better understanding of the influence of operating conditions, i.e. water height and floating film, on Fe(II) oxidation rate, arsenic speciation and removal, which control natural attenuation process that takes place in many As-rich AMD. Such factors should be considered in future design of passive treatment systems. Water height appeared salient for controlling the Fe(II) oxidation rate, which is the basis of the natural attenuation of arsenic. The floating film that formed naturally under low flow regime limited the oxygen transfer to the biogenic precipitate, thus delaying Fe(II) oxidation. Water height also strongly affected the Fe(II) oxidation rate and subsequent As removal; a thin water layer running

across the biogenic precipitate maximized both oxygen diffusion and biofilm surface area per unit water volume, thus improving the Fe(II) oxidation rate. The initial arsenic oxidation state also affected the As removal and speciation in the neoformed solid phases; higher initial As(V) thus favoured As removal in the form of amorphous ferric arsenate. The stability of these phases upon long-term storage should be considered in a general waste management scenario. Such treatment constitutes a first step of a whole AMD treatment since acid pH remains to be neutralized and metal cations have to be removed before the effluent can be released in the environment. Calcite drains or biological treatment based on bacterial sulphate reduction might be promising as complementary processes.

Acknowledgements

The authors thank the IngECOST-DMA project (ANR-13-ECOT-0009), the OSU OREME and the Ecole Doctorale GAIA (PhD fellowship of Lidia Fernandez-Rojo) for the financial support. We thank Remi Freydier for ICP-MS analysis on the AETE-ISO platform (OSU OREME, University of Montpellier). Christophe Duperray and Yann Bordat from the Montpellier RIO Imaging microscopy platform are gratefully acknowledged for their kind assistance in cytometry. We also thank Luca Olivi from the XAFS beamline from the ELETTRA-synchrotron for his assistance and advices, as well as the staff of the SAMBA beamline at the SOLEIL synchrotron for their assistance in XAS experiments. Benoit Baptiste (IMPMC) is acknowledged for his help to achieve micro-XRF measurements. We thank Didier Cot, from the Institut Européen de Membranes for its assistance in the Scanning Electron Microscope. Blandine Savajols, from the University of Montpellier, is also thanked for her valuable contribution during their internships in the laboratory HydroSciences Montpellier.

References

Ahoranta, S.H., Kokko, M.E., Papirio, S., Özkaya, B., Puhakka, J.A., 2016. Arsenic removal from acidic solutions with biogenic ferric precipitates. Journal of Hazardous Materials 306, 124–32. doi:10.1016/j.jhazmat.2015.12.012

Asta, M.P., Ayora, C., Román-Ross, G., Cama, J., Acero, P., Gault, A.G., Charnock, J.M., Bardelli, F., 2010a. Natural attenuation of arsenic in the Tinto Santa Rosa acid stream (Iberian Pyritic Belt, SW Spain): The role of iron precipitates. Chemical Geology 271 (1–2), 1–12. doi:http://dx.doi.org/10.1016/j.chemgeo.2009.12.005

Asta, M.P., Ayora, C., Acero, P., Cama, J., 2010b. Field rates for natural attenuation of arsenic in Tinto Santa Rosa acid mine drainage (SW Spain). Journal of Hazardous Materials 177 (1–3), 1102–1111. doi:10.1016/j.jhazmat.2010.01.034

Asta, M.P., Kirk Nordstrom, D., Blaine McCleskey, R., 2012. Simultaneous oxidation of arsenic and antimony at low and circumneutral pH, with and without microbial catalysis. Applied Geochemistry 27 (1), 281–291. doi:http://dx.doi.org/10.1016/j.apgeochem.2011.09.002

Battaglia-Brunet, F., Dictor, M.-C., Garrido, F., Crouzet, C., Morin, D., Dekeyser, K., Clarens, M., Baranger, P., 2002. An arsenic(III)-oxidizing bacterial population: selection, characterization, and performance in reactors. Journal of Applied Microbiology 93 (4), 656–667. doi:10.1046/j.1365-2672.2002.01726.x

Battaglia-Brunet, F., Itard, Y., Garrido, F., Delorme, F., Crouzet, C., Greffie, C., Joulian, C., 2006. A simple biogeochemical process removing arsenic from a mine drainage water. Geomicrobiology Journal 23 (3–4), 201–211. doi:10.1080/01490450600724282

Beyenal, H., Lewandowski, Z., 2002. Internal and external mass transfer in biofilms grown at various flow velocities. Biotechnology Progress 18 (1), 55–61. doi:10.1021/bp010129s

Bhandari, N., Reeder, R.J., Strongin, D.R., 2011. Photoinduced oxidation of arsenite to arsenate on ferrihydrite. Environmental Science & Technology 45 (7), 2783–2789. doi:10.1021/es103793y

Brantner, J.S., Haake, Z.J., Burwick, J.E., Menge, C.M., Hotchkiss, S.T., Senko, J.M., 2014. Depth-dependent geochemical and microbiological gradients in Fe(III) deposits resulting from coal mine-derived acid mine drainage. Frontiers in Microbiology 5 (215), 1–15. doi:10.3389/fmicb.2014.00215

Brown, J.F., Jones, D.S., Mills, D.B., Macalady, J.L., Burgos, W.D., 2011. Application of a depositional facies model to an acid mine drainage site. Applied and Environmental Microbiology 77 (2), 545–554. doi:10.1128/aem.01550-10

Bruneel, O., Personné, J.C., Casiot, C., Leblanc, M., Elbaz-Poulichet, F., Mahler, B.J., Le Flèche, A., Grimont, P.A.D., 2003. Mediation of arsenic oxidation by *Thiomonas* sp. in acid-mine drainage (Carnoulès, France). Journal of Applied Microbiology 95 (3), 492–499. doi:10.1046/j.1365-2672.2003.02004.x

Burton, E.D., Bush, R.T., Johnston, S.G., Watling, K.M., Hocking, R.K., Sullivan, L.A., Parker, G.K., 2009. Sorption of arsenic(V) and arsenic(III) to schwertmannite. Environmental Science & Technology 43 (24), 9202–9207. doi: 10.1021/es902461x

Carlson, L., Bigham, J.M., Schwertmann, U., Kyek, A., Wagner, F., 2002. Scavenging of As from acid mine drainage by schwertmannite and ferrihydrite: a comparison with synthetic analogues. Environmental Science & Technology 36 (8), 1712–1719.

Casiot, C., Morin, G., Juillot, F., Bruneel, O., Personné, J.-C., Leblanc, M., Duquesne, K., Bonnefoy, V., Elbaz-Poulichet, F., 2003. Bacterial immobilization and oxidation of arsenic in acid mine drainage (Carnoulès creek, France). Water Research 37 (12), 2929–2936. doi:http://dx.doi.org/10.1016/S0043-1354(03)00080-0

Chen, C.-J., Jiang, W.-T., 2012. Influence of waterfall aeration and seasonal temperature variation on the iron and arsenic attenuation rates in an acid mine drainage system. Applied Geochemistry 27 (10), 1966–1978. doi:http://dx.doi.org/10.1016/j.apgeochem.2012.06.003

Cheng, H., Hu, Y., Luo, J., Xu, B., Zhao, J., 2009. Geochemical processes controlling fate and transport of arsenic in acid mine drainage (AMD) and natural systems. Journal of Hazardous Materials 165 (1–3), 13–26. doi:http://dx.doi.org/10.1016/j.jhazmat.2008.10.070

Debiec, K., Krzysztoforski, J., Uhrynowski, W., Sklodowska, A., Drewniak, L., 2017. Kinetics of arsenite oxidation by *Sinorhizobium* sp. M14 under changing environmental conditions. International Biodeterioration & Biodegradation 119, 476–485. doi:10.1016/j.ibiod.2016.10.049

DeSa, T. C., Brown, J.F., Burgos, W.D., 2010. Laboratory and field-scale evaluation of low-pH Fe(II) oxidation at Hughes Borehole, Portage, Pennsylvania. Mine Water and the Environment 29 (4), 239–247. doi:10.1007/s10230-010-0105-5

587 Eberl, H.J., Picioreanu, C., Heijnen, J.J., van Loosdrecht, M.C.M., 2000. A three-dimensional numerical study
588 on the correlation of spatial structure, hydrodynamic conditions, and mass transfer and conversion in biofilms.
589 Chemical Engineering Science 55 (24), 6209–6222. doi:10.1016/S0009-2509(00)00169-X

590 Egal, M., Casiot, C., Morin, G., Elbaz-Poulichet, F., Cordier, M.-A., Bruneel, O., 2010. An updated insight into
591 the natural attenuation of As concentrations in Reigous Creek (southern France). Applied Geochemistry 25 (12),
592 1949–1957. doi:http://dx.doi.org/10.1016/j.apgeochem.2010.10.012

593 Eggerichs, T., Opel, O., Otte, T., Ruck, W., 2014. Interdependencies between biotic and abiotic ferrous iron
594 oxidation and influence of pH, oxygen and ferric iron deposits. Geomicrobiology Journal 31 (6), 461–472.
595 doi:10.1080/01490451.2013.870620

596 Elbaz-Poulichet, F., Bruneel, O., Casiot, C., 2006. The Carnoulès mine. Generation of As-rich acid mine
597 drainage, natural attenuation processes and solutions for passive in-situ remediation, in: Difpolmine (Diffuse
598 Pollution from Mining Activities), Dec 2006, Montpellier, France. <hal-00184269>

599 Fukushi, K., Sasaki, M., Sato, T., Yanase, N., Amano, H., Ikeda, H., 2003. A natural attenuation of arsenic in
600 drainage from an abandoned arsenic mine dump. Applied Geochemistry 18 (8), 1267–1278.
601 doi:http://dx.doi.org/10.1016/S0883-2927(03)00011-8

602 Grathoff, G.H., Baham, J.E., Easterly, H.R., Gassman, P., Hugo, R.C., 2007. Mixed-valent Fe films
603 ("Schwimmeisen") on the surface of reduced ephemeral pools. Clays and Clay Minerals 55 (6), 635–643.
604 doi:10.1346/CCMN.2007.0550610

605 Grishin, S.I., Tuovinen, O.H., 1988. Fast kinetics of Fe^{2+} oxidation in packed-bed reactors. Applied and
606 Environmental Microbiology 54 (12), 3092–3100.

607 Hovasse, A., Bruneel, O., Casiot, C., Desoeuvre, A., Farasin, J., Héry, M., Van Dorsselaer, A., Carapito, C.,
608 Arsène-Ploetze, F., 2016. Spatio-temporal detection of the *Thiomonas* population and the *Thiomonas* arsenite
609 oxidase involved in natural arsenite attenuation processes in the Carnoulès acid mine drainage. Frontiers in Cell
610 and Developmental Biology 4 (3), 1–14. doi:10.3389/fcell.2016.00003

611 Hug, S.J., Leupin, O., 2003. Iron-catalyzed oxidation of arsenic(III) by oxygen and by hydrogen peroxide: pH-
612 dependent formation of oxidants in the Fenton reaction. Environmental Science & Technology 37 (12), 2734–
613 2742. doi:10.1021/es026208x

614 Jiang, Z., Li, P., Jiang, D., Wu, G., Dong, H., Wang, Y., Li, B., Wang, Y., Guo, Q., 2014. Diversity and
615 abundance of the arsenite oxidase gene *aioA* in geothermal areas of Tengchong, Yunnan, China. Extremophiles
616 18 (1), 161–170. doi:10.1007/s00792-013-0608-7

617 Kim, J.-Y., Davis, A.P., Kim, K.-W., 2003. Stabilization of available arsenic in highly contaminated mine
618 tailings using iron. Environmental Science & Technology 37 (1), 189–195. doi:10.1021/es020799+

619 Kleja, D.B., van Schaik, J.W.J., Persson, I., Gustafsson, J.P., 2012. Characterization of iron in floating surface
620 films of some natural waters using EXAFS. Chemical Geology 326, 19–26. doi:10.1016/j.chemgeo.2012.06.012

621 Larson, L.N., Sánchez-España, J., Kaley, B., Sheng, Y., Bibby, K., Burgos, W.D., 2014. Thermodynamic
622 controls on the kinetics of microbial low-pH Fe(II) Oxidation. Environmental Science & Technology 48 (16),
623 9246–9254. doi:10.1021/es501322d

624 Lawrence, R.W., Higgs, T.W., 1999. Removing and stabilizing As in acid mine water. Journal of The Minerals,
625 Metals & Materials Society (TMS) 51 (9), 27–29. doi:10.1007/s11837-999-0154-z

626 Leblanc, M., Achard, B., Ben Othman, D., Luck, J.M., Bertrand-Sarfati, J., Personné, J.C., 1996. Accumulation
627 of arsenic from acidic mine waters by ferruginous bacterial accretions (stromatolites). Applied Geochemistry 11
628 (4), 541–554. doi:http://dx.doi.org/10.1016/0883-2927(96)00010-8

629 Liu, M.S., Branion, R.M.R., Duncan, D.W., 1988. The effects of ferrous iron, dissolved oxygen, and inert solids
630 concentrations on the growth of *Thiobacillus ferrooxidans*. The Canadian Journal of Chemical Engineering 66
631 (3), 445–451. doi:10.1002/cjce.5450660315

632 Macías, F., Caraballo, M.A., Nieto, J.M., Rötting, T.S., Ayora, C., 2012. Natural pretreatment and passive
633 remediation of highly polluted acid mine drainage. Journal of Environmental Management 104, 93–100.
634 doi:http://dx.doi.org/10.1016/j.jenvman.2012.03.027

635 Maillot, F., Morin, G., Juillot, F., Bruneel, O., Casiot, C., Ona-Nguema, G., Wang, Y., Lebrun, S., Aubry, E.,
636 Vlaic, G., Brown Jr, G.E., 2013. Structure and reactivity of As(III)- and As(V)-rich schwertmannites and
637 amorphous ferric arsenate sulfate from the Carnoulès acid mine drainage, France: Comparison with biotic and
638 abiotic model compounds and implications for As remediation. Geochimica et Cosmochimica Acta 104, 310–
639 329. doi:http://dx.doi.org/10.1016/j.gca.2012.11.016

Michel, C., Jean, M., Coulon, S., Dictor, M.-C., Delorme, F., Morin, D., Garrido, F., 2007. Biofilms of As(III)-oxidising bacteria: formation and activity studies for bioremediation process development. Applied Microbiology and Biotechnology 77 (2), 457–467. doi:10.1007/s00253-007-1169-4

Michon, J., Dagot, C., Deluchat, V., Dictor, M.-C., Battaglia-Brunet, F., Baudu, M., 2010. As(III) biological oxidation by CAsO1 consortium in fixed-bed reactors. Process Biochemistry 45 (2), 171–178. doi:10.1016/j.procbio.2009.09.003

Morin, G., Juillot, F., Casiot, C., Bruneel, O., Personné, J.-C., Elbaz-Poulichet, F., Leblanc, M., Ildefonse, P., Calas, G., 2003. Bacterial formation of tooeleite and mixed arsenic(III) or arsenic(V)−iron(III) gels in the Carnoulès acid mine drainage, France. A XANES, XRD, and SEM study. Environmental Science & Technology 37 (9), 1705–1712. doi:10.1021/es025688p

Ohnuki, T., Sakamoto, F., Kozai, N., Ozaki, T., Yoshida, T., Narumi, I., Wakai, E., Sakai, T., Francis, A.J., 2004. Mechanisms of arsenic immobilization in a biomat from mine discharge water. Chemical Geology 212 (3–4), 279–290. doi:10.1016/j.chemgeo.2004.08.018

Ona-Nguema, G., Morin, G., Wang, Y., Foster, A.L., Juillot, F., Calas, G., Brown, G.E., 2010. XANES evidence for rapid arsenic(III) oxidation at magnetite and ferrihydrite surfaces by dissolved O_2 via Fe^{2+} -mediated reactions. Environmental Science & Technology 44 (14), 5416–5422. doi:10.1021/es1000616

Paikaray, S., 2015. Arsenic geochemistry of acid mine drainage. Mine Water and the Environment 34 (2), 181–196. doi:10.1007/s10230-014-0286-4

Puyate, Y., Rim-Rukeh, A., 2008. Some physico-chemical and biological characteristics of soil and water samples of part of the Niger Delta area, Nigeria. Journal of Applied Sciences and Environmental Management 12 (2), 135–141.

Quéméneur, M., Cébron, A., Billard, P., Battaglia-Brunet, F., Garrido, F., Leyval, C., Joulian, C., 2010. Population structure and abundance of arsenite-oxidizing bacteria along an arsenic pollution gradient in waters of the upper isle River Basin, France. Applied and Environmental Microbiology. 76 (13), 4566–4570. doi:10.1128/AEM.03104-09

Rait, R., Trumm, D., Pope, J., Craw, D., Newman, N., MacKenzie, H., 2010. Adsorption of arsenic by iron rich precipitates from two coal mine drainage sites on the West Coast of New Zealand. New Zealand Journal of Geology and Geophysics 53 (2–3), 177–193.

Reina, M., Portillo, M.C., Serrano Martín, L., Lucassen, E.C.H.E.T., Roelofs, J.G.M., Romero, A., González, J.M., 2015. The interplay of hydrological, chemical and microbial processes in the formation of iron-rich floating films in aquatic environments at a circumneutral pH. Limnetica 34 (2), 365–380.

Resongles, E., Le Pape, P., Fernandez-Rojo, L., Morin, G., Brest, J., Guo, S., Casiot, C., 2016. Routine determination of inorganic arsenic speciation in precipitates from acid mine drainage using orthophosphoric acid extraction followed by HPLC-ICP-MS. Analytical Methods 8, 7420–7426. doi:10.1039/c6ay02084d

Robbins, E.I., Rodgers, T.M., Alpers, C.N., Nordstrom, D.K., 2000. Ecogeochemistry of the subsurface food web at pH 0–2.5 in Iron Mountain, California, U.S.A. Hydrobiologia 433 (1/3), 15–23. doi:10.1023/A:1004050216537

Sánchez España, J., López Pamo, E., Santofimia Pastor, E., 2007. The oxidation of ferrous iron in acidic mine effluents from the Iberian Pyrite Belt (Odiel Basin, Huelva, Spain): Field and laboratory rates. Journal of Geochemical Exploration 92 (2–3), 120–132. doi:http://dx.doi.org/10.1016/j.gexplo.2006.08.010

Savić, D.S., Veljković, V.B., Lazić, M.L., Vrvić, M.M., Vučetić, J.I., 1998. Effects of the oxygen transfer rate on ferrous iron oxidation by *Thiobacillus ferrooxidans*. Enzyme and Microbial Technology 23 (7), 427–431. doi:10.1016/S0141-0229(98)00071-4

Sheng, Y., Bibby, K., Grettenberger, C., Kaley, B., Macalady, J.L., Wang, G., Burgos, W.D., 2016. Geochemical and temporal influences on the enrichment of acidophilic iron-oxidizing bacterial communities. Applied and Environmental Microbiology 82 (12), 3611–3621. doi:10.1128/AEM.00917-16

van Veen, W.L., Mulder, E.G., Deinema, M.H., 1978. The *Sphaerotilus-Leptothrix* group of bacteria. Microbiological Reviews 42 (2), 329–356.

Volant, A., Bruneel, O., Desoeuvre, A., Héry, M., Casiot, C., Bru, N., Delpoux, S., Fahy, A., Javerliat, F., Bouchez, O., Duran, R., Bertin, P.N., Elbaz-Poulichet, F., Lauga, B., 2014. Diversity and spatiotemporal dynamics of bacterial communities: physicochemical and other drivers along an acid mine drainage. FEMS Microbiology Ecology 90 (1), 247–263. doi:10.1111/1574-6941.12394

Wan, J., Klein, J., Simon, S., Joulian, C., Dictor, M.-C., Deluchat, V., Dagot, C., 2010. AsIII oxidation by *Thiomonas arsenivorans* in up-flow fixed-bed reactors coupled to As sequestration onto zero-valent iron-coated sand. Water Research 44 (17), 5098–5108. doi:10.1016/j.watres.2010.08.044

695 Wäsche, S., Horn, H., Hempel, D.C., 2002. Influence of growth conditions on biofilm development and mass
696 transfer at the bulk/biofilm interface. Water Research 36 (19), 4775–4784. doi:10.1016/S0043-1354(02)00215-4

697 Williams, M., 2001. Arsenic in mine waters: an international study. Environmental Geology 40 (3), 267–278.
698 doi:10.1007/s002540000162

699 Wilmes, P., Remis, J.P., Hwang, M., Auer, M., Thelen, M.P., Banfield, J.F., 2009. Natural acidophilic biofilm
700 communities reflect distinct organismal and functional organization. The ISME Journal 3 (2), 266–270.
701 doi:10.1038/ismej.2008.90

TABLES

Table 1. Inlet water chemistry for the whole duration of the experiments. In Exp 1 $_{(OA)}$ the channels were fed for 17 days with the water collected on 20/01/2015, followed by 14 days with the water collected on 12/02/2015. SD = standard deviation, n= number of samples. Fe(II), Total Fe, As(III), As(V), Total As are concentrations in the dissolved phase.

Code	Experimental conditions	Date of water collection	Experiment duration (days)		pH	T (°C)	EC (mS cm^{-1})	Eh (mV)	Fe(II) (mg L^{-1})	Total Fe (mg L^{-1})	As(III) (mg L^{-1})	As(V) (mg L^{-1})	Total As (mg L^{-1})	SO_4^{2-} (g L^{-1})
Exp 1 $_{(FF)}$	Water height: 4 mm Floating film: Yes Air bubbling: No	20/01/2015	17	Average	3.0	20	3.21	535	439	452	13	17	30	1.8
				SD	0.1	1	0.06	39	30	26	4	6	9	0.1
				SD (%)	2	3	2	7	7	6	32	36	31	5
				n	20	19	8	8	20	8	8	8	8	8
Exp 1 $_{(OA)}$	Water height: 4 mm Floating film: No Air bubbling: No	20/01/2015 + 12/02/2015	34	Average	3.1	19.7	3.0	547	432	441	19	12	31	1.8
				SD	0.2	0.5	0.2	34	29	23	8	7	7	0.1
				SD (%)	5	3	7	6	7	5	40	54	22	4
				n	27	25	15	15	27	15	15	15	15	15
Exp 2 $_{(4\ mm)}$	Water height: 4 mm Floating film: No Air bubbling: No	23/03/2015	35	Average	3.4	20.0	2.89	499	480	484	30	6	36	1.9
				SD	0.3	0.8	0.06	45	25	19	10	2	10	0.1
				SD (%)	9	4	2	9	5	4	34	42	29	6
				n	35	35	22	23	35	15	18	18	18	15
Exp 2 $_{(25\ mm)}$	Water height: 4 mm (22 days) + 25 mm (13 days) Floating film: No Air bubbling: No	23/03/2015	35	Average	3.4	19.8	2.89	494	476	482	33	6	39	1.9
				SD	0.3	0.8	0.06	46	29	16	12	2	11	0.1
				SD (%)	10	4	2	9	6	3	37	40	30	3
				n	28	28	16	16	28	8	11	11	11	8
Exp 2 $_{(25\ mm,\ Air)}$	Water height: 4 mm (22 days) + 25 mm (13 days) Floating film: No Air bubbling: last 6 days	23/03/2015	35	Average	3.4	19.8	2.87	492	472	479	33	5	38	1.9
				SD	0.3	0.8	0.07	48	29	13	12	2	12	0.1
				SD (%)	10	4	2	10	6	3	37	41	31	4
				n	28	28	16	16	28	8	11	11	11	8

Table 2. Average Fe(II) oxidation rate, total Fe precipitation rate, and total As, As(III) and As(V) removal rates calculated within the range of residence times 20-500 minutes during kinetic studies.

	Fe(II) oxidation rate (mol L^{-1} s^{-1})	Total Fe precipitation rate (mol L^{-1} s^{-1})	Total As removal rate (mol L^{-1} s^{-1})	As(III) removal rate (mol L^{-1} s^{-1})	As(V) removal rate (mol L^{-1} s^{-1})
Exp 1 (FF)	$3 \pm 2 \times 10^{-7}$	$1.2 \pm 0.9 \times 10^{-7}$	$5 \pm 4 \times 10^{-8}$	$8 \pm 6 \times 10^{-9}$	$5 \pm 4 \times 10^{-8}$
Exp 1 (OA)	$4.4 \pm 0.6 \times 10^{-7}$	$2.4 \pm 0.5 \times 10^{-7}$	$5 \pm 2 \times 10^{-8}$	$3 \pm 2 \times 10^{-8}$	$1.2 \pm 0.9 \times 10^{-8}$
Exp 2 (4 mm)	$2.7 \pm 0.5 \times 10^{-7}$	$1.3 \pm 0.2 \times 10^{-7}$	$2 \pm 2 \times 10^{-8}$	$2 \pm 1 \times 10^{-8}$	$7 \pm 6 \times 10^{-9}$
Exp 2 (25 mm)	$4 \pm 3 \times 10^{-8}$	$1.8 \pm 0.9 \times 10^{-8}$	$5 \pm 3 \times 10^{-9}$	$2 \pm 2 \times 10^{-9}$	$3 \pm 2 \times 10^{-9}$

Table 3. Characterization of the biogenic precipitates recovered from the channel bottom at the end of experiments and of the floating film from Exp 1 $_{(FF)}$. SD = standard deviation, n= number of samples, Schwert. = Schwertmannite. Exp 1 $_{(FF)}$, Exp 1 $_{(OA)}$, and Exp 2 $_{(4\ mm)}$ have two experiment replicates (Referred as channel 1 and channel 2 in figures in the SI). Exp 2 $_{(25\ mm)}$ and Exp 2 $_{(25\ mm,\ Air)}$ have been conducted in a single channel. Results from As K-edge XANES (Resongles et al., 2016), As K-edge EXAFS and Fe K-edge EXAFS are normalized to 100%. Non-normalized results are reported in Table SI-2 and SI-3, together with uncertainties on the proportion of each component.

		Flow citometry	qPCR	Acid Digestion			XRD	As K-edge XANES		As bearing phases (As K-edge EXAFS)			Fe bearing phases (Fe K-edge EXAFS)	
		Cells g^{-1} (dry wt.)	*aioA*/16S rRNA gene ratio	Total As % (dry wt.)	Total Fe % (dry wt.)	As/Fe molar ratio	Mineralogy	As(III) %	As(V) %	Schwert.-As (III) %	Schwert.-As(V) %	Amorphous ferric arsenate %	Schwert. %	Amorphous ferric arsenate %
Exp 1 (FF) Biogenic precipitate	Average	8 x 10^6	0.10	8	35	0.18	Schwert.	16	84	16	22	62	67	33
	SD	2 x $10^{6\ a}$	0.01[a]	1	0	0.01		2[c]	2[c]	2[c]	7[c]	65[c]	13[c]	5[c]
	n	6	5	2	2	2	2	1	1	1	1	1	1	1
Floating film	Average	n.d.	n.d.	n.d.	n.d.	n.d.	n.d.	n.d.	n.d.	27	22	51	78	22
	SD									3[c]	10[c]	9[c]	12[c]	5[c]
	n									1	1	1	1	1
Exp 1 (OA) Biogenic precipitate	Average	3 x 10^6	0.26	8	34	0.18	Schwert.	23	77	23	38	39	77	23
	SD	1 x $10^{6\ a}$	0.05[a]	1	0	0.00		2	2	3	17	20	7	3
	n	6	6	2	2	2	2	2	2	2	2	2	2	2
Exp 2 (4 mm) Biogenic precipitate	Average	9 x 10^6	0.3	6.3	36	0.14	Schwert.	52	48	51	18	31	85	15
	SD	5 x $10^{6\ a}$	0.3[a]	0.4	0	0.00		3	3	4	4	0	11[c]	3[c]
	n	6	6	2	2	2	2	2	2	2	2	2	1	1
Exp 2 (25 mm) Biogenic precipitate	Average	4.4 x 10^6	0.36	8	35	0.20	Schwert.	31	69	29	16	55	68	32
	SD	0.6 x $10^{6\ a}$	0.05[b]	1[b]	0[b]	0.00[b]		2[c]	2[c]	2[c]	2[c]	7[c]	5[c]	3[c]
	n	3	1	1	1	1	1	1	1	1	1	1	1	1
Exp 2 (25 mm, Air) Biogenic precipitate	Average	3 x 10^6	0.24	8	36	0.16	Schwert.	46	54	44	20	36	81	19
	SD	1 x $10^{6\ a}$	0.05[b]	1[b]	0[b]	0.00[b]		2[c]	2[c]	2[c]	7[c]	6[c]	11[c]	3[c]
	n	3	1	1	1	1	1	1	1	1	1	1	1	1

n.d.= not determined

a. calculated from DNA extraction replicates and from experimental replicates

b. analytical uncertainty

c. SD of the LCF obtained with the Athena Software, multiplied by a factor of 3 (see SI-Experimental part for details)

Other SD values were calculated from experimental replicates

721

722

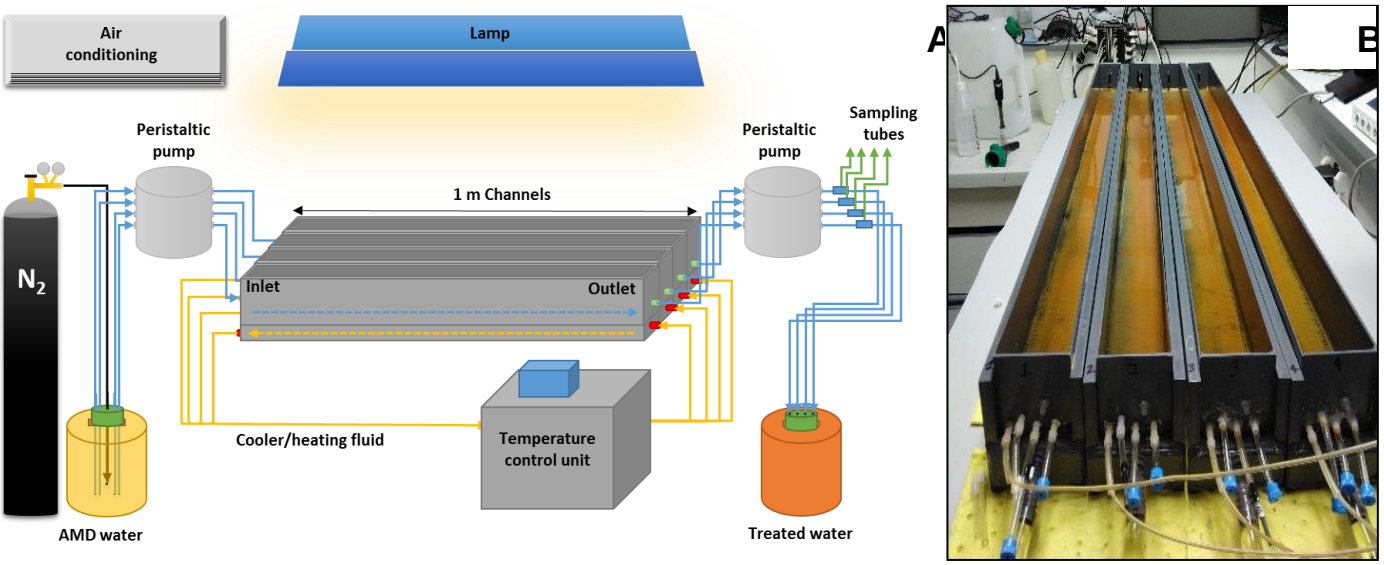

723

724 **Figure 1**. Schematic representation of the continuous flow bioreactor simulating natural
725 attenuation (A). The four channels fed with AMD and covered with the Fe-As biogenic precipitates at
726 the bottom (B).

727

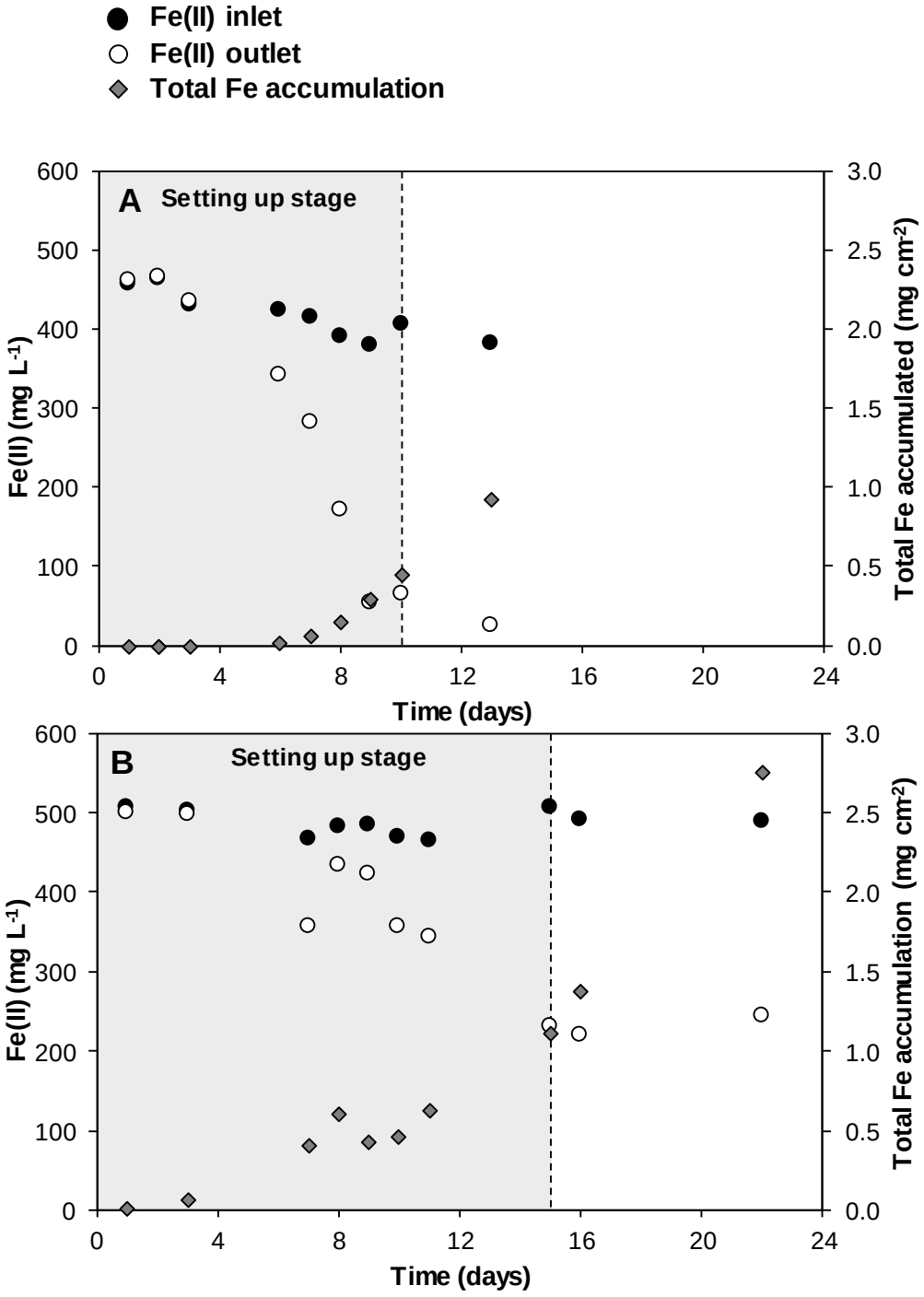

728

729 **Figure 2**. Dissolved Fe(II) concentration in the inlet and outlet waters and cumulated precipitated
730 Fe (expressed as mass of Fe precipitated per surface area of the channel bottom) during setting up
731 stage of experiments (A) Exp 1 and (B) Exp 2. Dashed line represents the period after which the
732 steady-state was reached regarding outlet Fe(II) concentration : ~10 days in Exp 1 and ~15 days in Exp
733 2.

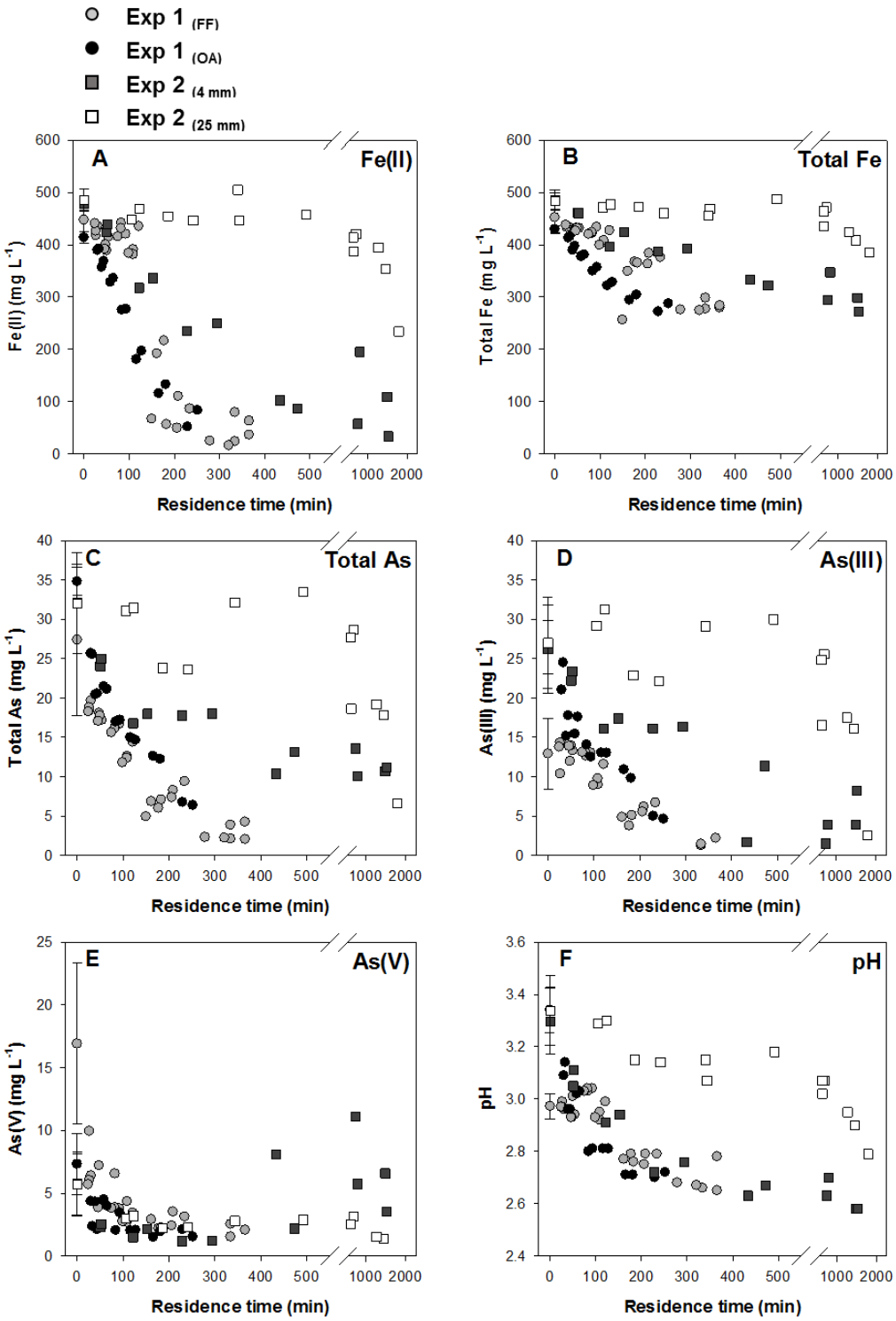

Figure 3. Water composition at the outlet of the flow reactor as a function of residence time during kinetic studies. Variation of dissolved Fe(II) (A), total dissolved Fe (B), total dissolved As (C), dissolved As(III) (D), dissolved As(V) (E) and pH (F) as a function of residence time during kinetic studies, carried out once steady-state condition was reached. Exp 1 $_{(FF)}$ (four replicate channels), Exp 1 $_{(OA)}$ (two replicate channels), and Exp 2 (Exp 2 $_{(4\ mm)}$ and Exp 2 $_{(25\ mm)}$, two replicate channels for each water height) were carried out with water from the Carnoulès AMD collected on 20th January, 12th February, and 23th March respectively. The corresponding values of Fe(II) oxidation rate, Fe and As

742 precipitation rates, As(III) and As(V) removal rates within the range of residence times 30 – 500
743 minutes are stated in Table 2.

744

745

746

747

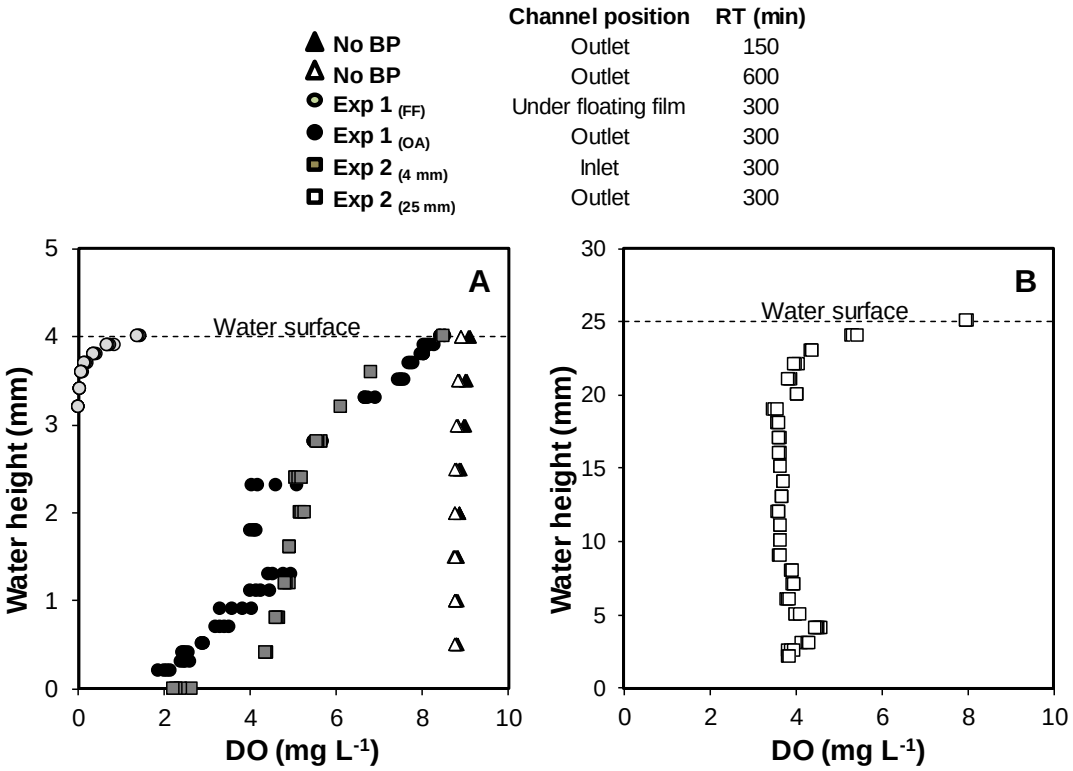

748
749 **Figure 4**. DO concentration profiles recorded in experiments conducted at 4 mm (A) and at 25 mm
750 (B). BP = biogenic precipitate.

751

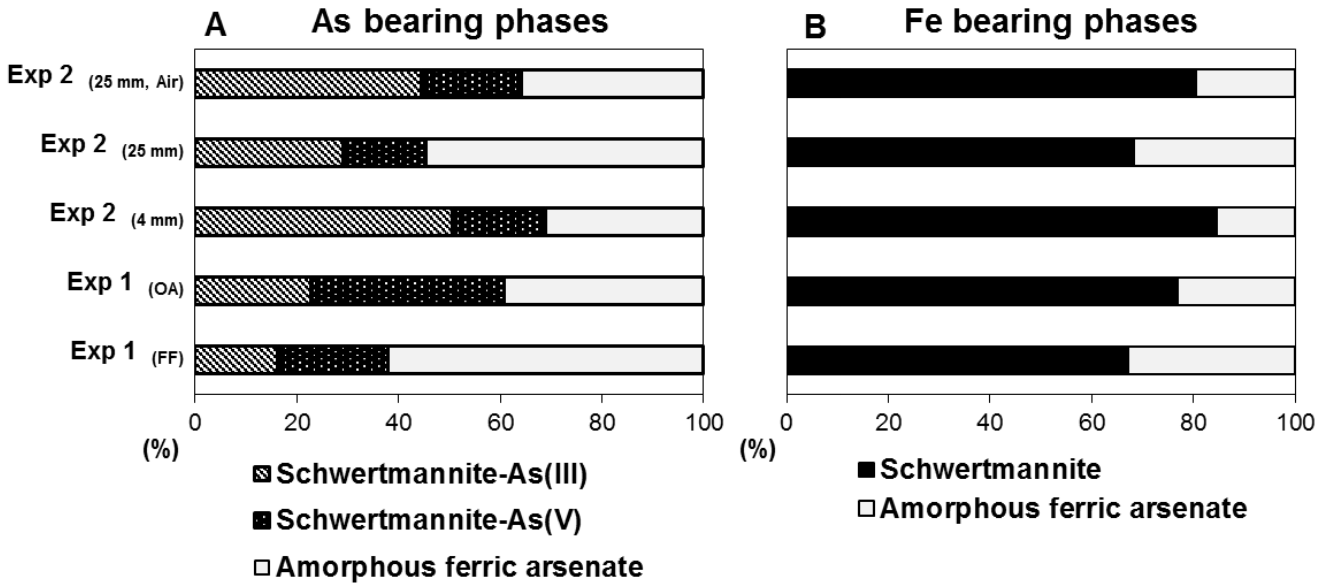

752 **Figure 5.** Arsenic speciation and mineralogy in the biogenic precipitates determined by LCF
753 analysis of As (A) and Fe K-edge (B) EXAFS data, respectively. Corresponding spectra are displayed
754 in Figures SI-3 and SI-4, respectively. LCF results are reported in Tables SI-2 and SI-3, respectively.

755

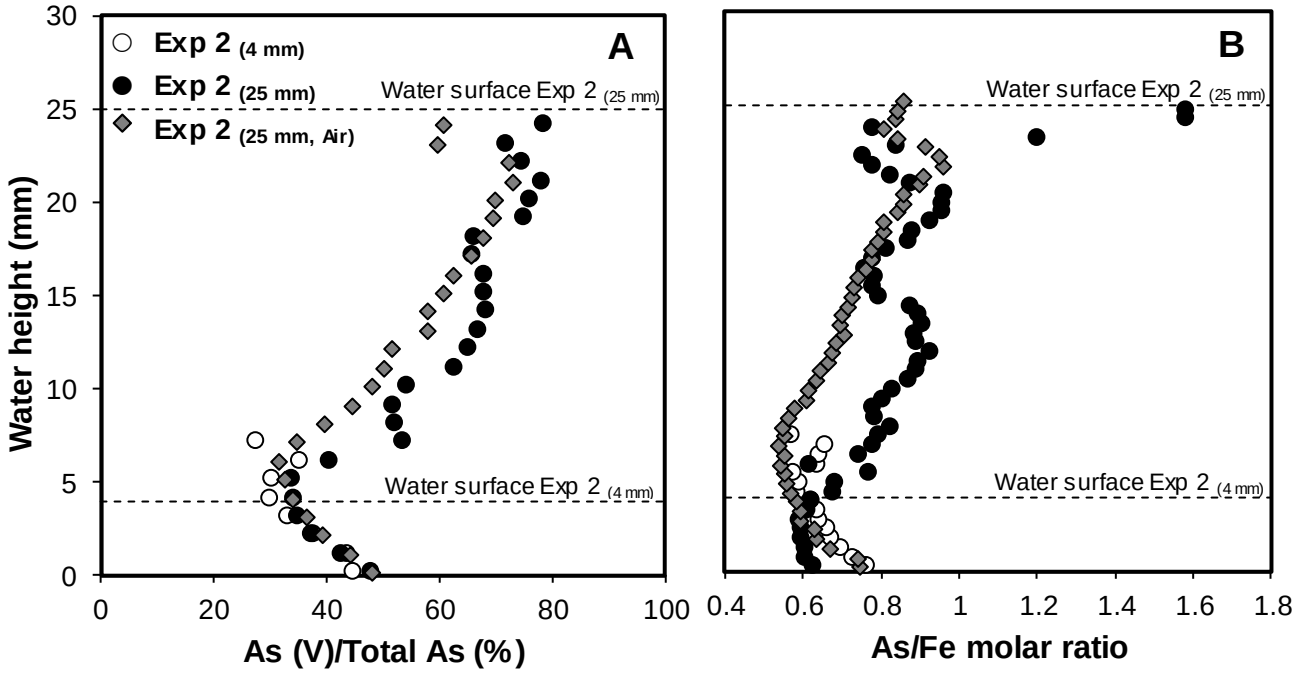

756

757 **Figure 6.** Normalized proportion of As(V)/Total As obtained by micro-XANES (A) and molar
758 ratio of As/Fe obtained by and micro-XRF (B) in the precipitate deposited on the plastic film inserted
759 vertically in the water column, in Exp 2 $_{(4\ mm)\text{-}channel\ 2}$, Exp 2 $_{(25\ mm)}$ and Exp 2 $_{(25\ mm,\ Air)}$.

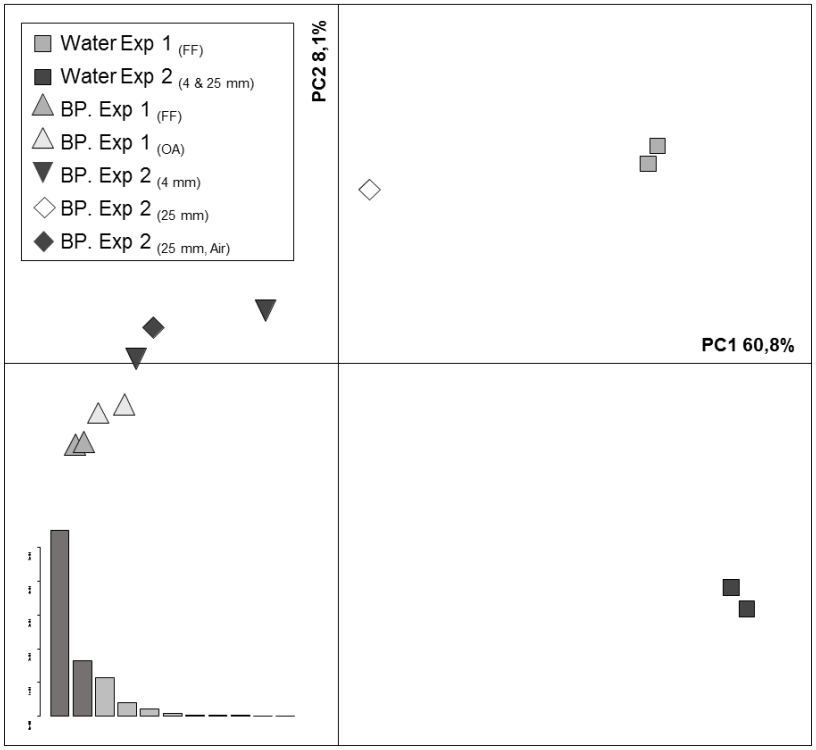

Figure 7. Principal component analysis plot generated from ARISA profiles obtained from the bacterial communities of water used in Exp 1 $_{(FF)}$ and in Exp 2 $_{(4\ mm\ \&\ 25\ mm)}$, and those of the biogenic precipitates (BP) formed at the bottom of the channels recovered at the end of the experiments: Exp 1 $_{(FF)}$, Exp 1 $_{(OA)}$, Exp 2 $_{(4\ mm)}$, Exp 2 $_{(25\ mm),}$ and Exp 2 $_{(25\ mm,\ Air)}$. Legend is shown in the upper left corner. Percentages of variance of all axes are shown in the lower left corner. The first component (PC1) represented 60.8 % of the bacterial community variability and indicates that the bacterial community in the biogenic precipitates differed widely from the bacterial community in the corresponding feed water. The second component (PC2) represented 8.1 %, of the bacterial community variability and highlights the variability between the feed waters.

SUPPORTING INFORMATION FILE

Biological attenuation of arsenic and iron in Acid Mine Drainage (AMD) in a continuous flow reactor

Fernandez-Rojo L.[1], Héry M.[1], Le Pape P.[2], Braungardt C.[3,1], Desoeuvre A.[1], Torres E.[1], Tardy V.[1], Resongles E.[1], Laroche E.[1], Delpoux S.[1], Joulian C.[4], Battaglia-Brunet F.[4], Boisson J.[5], Grapin G.[6], Morin G.[2], Casiot C.[1]

[1] Hydrosciences Montpellier, UMR 5569 CNRS-IRD-UM, CC57, 163, rue Auguste Broussonet, 34090, Montpellier, France

[2] Institut de Minéralogie, de Physique des Matériaux et de Cosmochimie (IMPMC), *UMR 7590 CNRS-UPMC-IRD-MNHN,*, 4 place Jussieu, 75252 Paris cedex 05, France

[3] School of Geography, Earth and Environmental Sciences (Faculty of Science & Engineering), Plymouth University, United Kingdom

[4] French Geological survey (BRGM), 3 avenue Claude Guillemin, 45060, BP 36009, Orléans Cedex, France

[5] IRH Ingénieur Conseil, 197 avenue de Fronton, 31200, Toulouse, France

[6] IRH Ingénieur Conseil, 427 rue Lavoisier - CS 50155, 54714, Ludres Cedex, France

1. **SI-EXPERIMENTAL PART**
2. **Chemical analysis**

2.1 Water chemistry analysis

Each water sample collected in the bioreactor was divided in two sub-samples. In one sub-sample, pH, conductivity and redox potential were determined with a multiparameter analyzer (UltrameterTM Model 6P) equipped with the specific electrodes. DO and temperature were measured directly within the channel. An oxygen microoptode (50 µm tip diameter, Unisense, DL = 0.01 mg L^{-1}), coupled to a microoptode-meter and fixed in a micromanipulator, was used to record dissolved oxygen depth profiles in the water column. The second sub-sample was immediately filtered using syringes (20 mL, Low Density Polyethylene, Codan) and disposable syringe filters (cellulose acetate, pore size 0.2 µm). The filtrate was distributed between four polypropylene tubes of 10 mL and preserved according to the procedures adapted to each analyte of interest (Fe(II), sulphate, total Fe and As, and As speciation) (Casiot *et al*., 2003; Héry *et al*., 2014; Resongles *et al*., 2014), as described below.

All the reagents used were Merck Suprapur® quality. For total Fe and As analyses, a 2.5 mL aliquot was acidified with HNO_3 (Suprapur) to pH 1 and stored at 4 °C. For Fe(II) determination, a 50 µL aliquot was buffered to pH 4.5 with 0.5 mL of ammonium acetate/acetic acid buffer and the Fe (II) was complexed with 1 mL of 0.5 % (w/w) 1,10-phenantroline chloride solution (Rodier *et al*., 1996). The tube was completed with 8.45 mL of double deionized water (DDW), and stored at 4 °C in the dark. For sulphate determination, a 100 µL aliquot was stabilized with 200 µL of HCl 10 % (v/v). Two millimetres of $BaCl_2$ solution were added and made up to 10 mL with DDW. For As speciation, 25 µL of EDTA (0.13 M) and 25 µL of acetic acid (8.7 M) were added to 2.5 mL sample and stored at 4 °C until analysis within less than 8 weeks.

For each analysis, the detection limit was calculated by multiplying by three the standard deviation of the blank, and the uncertainty was checked by repeating the measure of the Certified Reference Material (CRM) ten times and by calculating the relative standard deviation (RSD). Analysis of total Fe and As in water were carried out by inductively coupled plasma-mass spectrometer (ICP-MS; iCAP™ Q, Thermo Scientific, As detection limit = 0.03 µg L^{-1}, Fe detection limit = 0.3 µg L^{-1}, uncertainty = ± 1 %), after preparing the appropriate dilutions. The certified reference water SLRS-5 (CNRC Canada) was used to check the analytical accuracy and the RSD was always lower than 5 % with respect to the certified value. Spectrophotometric methods (SECOMAN S250) were used to determine Fe(II) (wave length (λ) = 510 nm, detection limit = 88 µg L^{-1}, uncertainty = ± 5 %) and sulfate (λ = 650 nm, detection limit = 1000 µg L^{-1}, uncertainty = ± 5 %). Fe and SO_4^{2-} standards (1000 mg L^{-1}, SCP Science), respectively, were used for calibrations. Samples were diluted for As speciation analysis and analysed using high performance liquid chromatography (HPLC)-ICP-MS with an anion exchange column (25 cm × 4.1 mm i.d. Hamilton PRP-X100) coupled to the ICP-MS (XSERIES II, Thermo Scientific, detection limit = 0.2 µg L^{-1} for As(III) and 0.4 µg L^{-1} for As(V), uncertainty = ± 5 %), The certified reference water NIST1643e was used to check analytical accuracy for total As concentration and the RSD was always lower than 5 % with respect to the certified value.

2.2 Sediment acid digestion

All reagents were of analytical grade and all material was decontaminated with HNO_3 (10 %) before starting. Solid samples were dried under vacuum at ambient temperature. One hundred milligrams of dried sample were introduced in 30 mL Teflon reactors placed on hot-plates. Samples were first attacked for 24 h with 3 mL H_2O_2 (30 % w/w) and then with aqua regia (3 mL HCl (35 % w/w), 1 mL HNO_3 (67 % w/w)) for 24 h more. After each attack, the solution was evaporated until the sample was dry. Subsequently, trace elements were dissolved in 3 mL HNO_3 (67 % w/w) and 27 mL of DDW. If necessary, appropriate dilutions with HNO_3 (2% (v/v)) were carried out before analysis with ICP-MS (same procedure as described above in "water chemistry analysis"). A certified reference material (Stream sediments LGC6189 from United Kingdom Accreditation Service and NCS DC70317 from LGC Standards, number of extractions = 3) was used to assess the extraction quality with recoveries of 108 ± 5 % for As (Fe concentration not referenced). Two blanks were prepared in each digestion and its concentration represented always less than 1 % with respect to Fe and As concentrations from samples.

2.3 Arsenic mass balance

At the end of each experiment, a mass balance was calculated in an attempt to determine in a qualitative way whether As(III) oxidation took place in the channels during the whole experiment. The trapezoidal rule was applied to calculate the defined integrals of inlet and outlet As(III), As(V) and total As load (mg s^{-1}) over the duration of the experiment. The difference between inlet and outlet load provided the masses of As(III) and As(V) removed from the dissolved phase during the whole experiment, which were compared with the masses of As(III) and As(V) determined in the precipitates at the end of the experiments.

3. Mineralogical analysis

Before mineralogical analysis, the aliquots of the biogenic precipitate samples recovered in the channels were deposited on silicon single-crystal low-background sample holders and dried under anoxic atmosphere in a Jacomex® anaerobic chamber filled with argon to avoid As(III) oxidation.

3.1 X-Ray diffraction (XRD)

XRD measurements were performed using the Co Kθ radiation of a Panalytical®X'Pert Pro diffractometer. Data were then collected in continuous mode between 5 and 100°2θ with a 0.033°2θ step, counting around 4 h per sample.

3.2 Extended X-ray absorption fine structure (EXAFS) spectroscopy

Both, As and Fe K-edge EXAFS spectra for the biogenic precipitate samples recovered in the channels of the experimental bioreactor system were recorded at 80 K in transmission mode on the XAFS beamline (ELETTRA, Trieste, Italy) using a Si(111) double-crystal monochromator. To preserve the As redox, status samples were mounted on the cryostat sample rod within a glovebox next to the beamline and quickly transferred into the cryostat. The incident beam energy was calibrated by setting to 11947 eV the energy position of the absorption maximum in the L_{III}-edge of an Au foil recorded in double-transmission for As, and by setting to 7112 eV the energy position of the absorption maximum in the K-edge of a Fe(0) foil for Fe. Up to two scans were recorded for each sample depending on As and Fe concentrations, i.e. on signal to noise ratio.

Scans were averaged, normalized and background subtracted over the 0–15 $Å^{-1}$ k-range for As and over the 0–14 $Å^{-1}$ k-range for Fe using the Athena Software (Ravel and Newville, 2005). Linear combination fitting (LCF) of EXAFS data was performed on k^3-weighted curves over the 3–15 $Å^{-1}$ k-range for As and the 2–14 $Å^{-1}$ k-range for Fe.

EXAFS data at both the As and Fe K-edges were interpreted by comparison with a large set of iron arsenic hydroxysulfate amorphous and nano-crystalline phases already analysed in detail by Maillot *et al*. (2013). These model compounds includes biotic and abiotic sorption and coprecipitation samples for As(III) and As(V) with various As/Fe molar ratios. Experimental spectra of three of these compounds, namely: As(III)-coprecipitated schwertmannite with As/Fe = 0.2 mol/mol (As3_02), As(V)-sorbed schwertmannite with As/Fe = 0.01 mol/mol (As5_ads) and Amorphous Ferric Arsenate with As/Fe = 0.8 mol/mol (As5_0.8) were used as fitting components for LCF analysis of the As K-edge EXAFS spectra of the biogenic precipitates. Indeed, these compounds reliably represent the variety of local structures encountered in such AMD precipitates and that can be distinguished by EXAFS at the As K-edge (Maillot *et al*. 2013). In the same way, As-free schwertmannite (As Free), As(III)-coprecipitated schwertmannite with As/Fe = 0.2 mol/mol (As3_02), and amorphous ferric arsenate with As/Fe = 0.8 mol/mol (As5_0.8) were used as fitting components for LCF analysis of the Fe K-edge EXAFS spectra.

3.3 Spatially resolved X-ray absorption near fine structure (XANES) measurements on plastic films

As K-edge XANES spectra on mineralized plastic films recovered in the channels of the experimental bioreactor system were collected at 15 K in fluorescence mode on the SAMBA beamline (SOLEIL, Saint-Aubin, France) using a Si(220) double-crystal monochromator and a 30 element Ge detector. XANES measurements were collected from the bottom to the top of the plastic films with a 1 mm step with a sample holder specially designed for this purpose. Beam size for the XANES measurements was approximately 0.25 mm vertically and 0.5 mm horizontally.

XANES linear combination fits (LCF) using As(III) and As(V) model compounds were performed using a in-house program based on a Levenberg–Marquardt algorithm. Model compounds used to fit the experimental spectra were As(III) and As(V) coprecipitated schwertmannites. Details about those compounds and data processing procedures can be found in Resongles *et al*. (2016).

3.4 Micro-X-ray fluorescence on plastic films

Micro X-ray fluorescence measurements were performed using a RIGAKU® Mo Kα rotating anode source collimated to 50 × 70 μm^2. For this experiment, the vertical step size was approximately 0.1 mm, and measurements were performed with steps of 0.5 mm from the bottom to the top of the plastic films.

After obtaining the X-ray emission spectra, As/Fe molar ratio for each point on the plastic films was calculated using a homemade program that calculates and divides As area measured at the As Kα emission line by the Fe area measured at the Fe Kα emission line. Then the area ratio is weighted by the ratio of the absorption factors corresponding to these emission lines.

4. Microbiological analysis

4.1 Bacterial quantification by flow cytometry

4.1.1 Bacterial quantification in water

Bacterial cells were pelleted by centrifugation (15 min at 6000 *g*, VWR® Mini Centrifuge) and resuspended into 50 µL of the same water. Bacterial cells were then stained (LIVE/DEAD® BacLigh Bacterial Viability Kits, Life Technologies) according to the manufacturer recommendations. Stained cells were counted automatically using a Gallios™ flow cytometer (Beckman Coulter) and data were analyzed with the Gallios software. More than 20,000 analytical events were counted, in triplicate, for each sample.

4.1.2 Bacterial quantification in the biogenic precipitate

Bacteria from recovered biogenic precipitates were detached from their particle-association according to the procedure described by Lunau *et al*. (2005) with some modifications. Briefly, the biogenic precipitate was sonicated (15 min, Transsonic 275 Prolabo) with 10 % methanol and centrifuged (1 min at 190 *g*, VWR® Mini Centrifuge) to remove detrital and inorganic particles. The supernatant containing suspended bacterial cells was centrifuged (15 min at 6000 *g*) and the resulting pellet was washed with 1 mL of sterile water, centrifuged again (15 min at 6000 *g*) and the supernatant discarded. Bacteria were stained and directly counted as described in the previous section “bacterial quantification in water”.

4.2 Bacterial community structure analysis by automated ribosomal intergenic spacer analysis (ARISA)

4.2.1 Bacterial community structure analysis in water

Total DNA was extracted from two of the three filters using the Power water® DNA Isolation kit (Mobio Laboratories) according to the manufacturer recommendations. The bacterial ribosomal intergenic regions were amplified by polymerase chain reaction (PCR) from the DNA extracts using primers ITSF and ITSR according to Cardinale *et al*. (2004). ARISA was performed on an Agilent 2100 Bioanalyzer using the 7500 DNA kit (Agilent Technologies). Principal component analysis (PCA) was performed from the ARISA profiles with the R free software (http://www.r-project.org/) and ade4 package.

4.2.2 Bacterial community structure analysis in the biogenic precipitate

Because sample acidity can interfere with the DNA extraction protocol, aliquots of the biogenic precipitate recovered from the bottom of the channels (~300 mg) were washed with 1 mL Tris-HCl (1 M, pH 8) to increase the pH of the sample. Then DNA was extracted using an UltraClean Soil DNA Isolation Kit (MOBIO Laboratories), according to the manufacturer's instructions. Up to three DNA replicates extractions were made on one sample. The bacterial community structures (ARISA profiles) were determined as described above in "bacterial community analysis in water".

4.3 16S rRNA and aioA genes quantification in the biogenic precipitate

The abundance of *aioA* genes, encoding the large catalytic subunit of the As(III) oxidase, was determined by quantitative *real-time* PCR (qPCR) in each DNA replicate extract of samples recovered from the biogenic precipitates (DNA extraction protocol described in "bacterial community structure analysis in the biogenic precipitate"). The reverse primer aoxBM2-1R (5'-GGAGTTGTAGGCGGGCCKRTTRTGDAT-3') (Quéméneur *et al*., 2010) was combined with the forward primer aoxBM4-1F (5'-TTCTGCATCGTGGGCTGYGGNTAYMA-3') to target a 110 bp fragment of the *aioA* gene (Quéméneur, 2008). Each primer was used at a concentration of 0.3 µM, with 100 ng of T4GP32 (MP Biomedicals), in 1X IQ SYBR Green Supermix (BioRad) and a final volume of 20 µL. Two microliters of DNA, diluted at 1 ng μL^{-1} when appropriate, were used as template. The program was run in a CFX Connect (BioRad) and consisted in an initial denaturation at 95 °C for 3 min, followed by 45 cycles of 95 °C for 10 s, 54 °C for 20 s, 72 °C for 10 s, and a data acquisition step at 80 °C for 10 s. At the end, a melting curve analysis was performed through measurement of the SYBR Green I signal intensities during a 0.5 °C temperature increment every 10 s, from 65 °C to 95 °C. Negative controls received 2 µL of ultra-pure water (MP Biomedicals) instead of DNA. Total *Bacteria* abundance was measured by qPCR on the 16S rRNA gene using universal bacterial primers 341F (5′-CCTACGGGAGGCAGCAG-3′) and 534R (5′-ATTACCGCGGCTGCTGGCA-3′), as previously described (López-Gutiérrez *et al*., 2004). Six-point serial decimal dilution of a linearized plasmid carrying the target gene (*aioA* or 16S rRNA gene) was used to generate a linear calibration curve of threshold cycle versus a number of gene copies ranging from 10^2 to 10^7. All measurements were run in duplicates.

5. TABLES

Table SI-1. Equivalence of samples names in this paper and in Resongles *et al.*, (2016), which includes the methodology and results of the As K-edge XANES data, also presented in this study.

Resongles et al., (2016)	This study
1A-G4	Exp 1 $_{(FF)}$ - Channel 2
1B-G1	Exp 1 $_{(OA)}$ - Channel 1
1B-G2	Exp 1 $_{(OA)}$ - Channel 2
2A-G2	Exp 2 $_{(4\ mm)}$ - Channel 1
2A-G4	Exp 2 $_{(4\ mm)}$ - Channel 2
2A-G3	Exp 2 $_{(25\ mm)}$
2A-G1	Exp 2 $_{(25\ mm,\ Air)}$

Table SI-2. Results of the linear combination fitting (LCF) procedure (non-normalized data) applied to As K-edge EXAFS of the biogenic precipitate and floating film samples. LCF were performed using the Athena Software on the 3–15 $Å^{-1}$ k-range. The fitted contributions of the As species are reported in percentages, without normalizing the sum to 100%. The model compounds used for the LCF procedure consisted of As(III)-coprecipitated schwertmannite "As3_0.2", As(V)-sorbed shcwertmannite "As5_ads", and ferric arsenate "As5_0.8" reported by Maillot *et al*. (2013). R-factor (R_f), chi-square (χ^2) and reduced chi-square (Red-χ^2) are given as classical estimators of the goodness of fit. Uncertainties on the contributions are given in parentheses and refer as 3 standard deviation (σ) obtained with the Athena Software. Experimental replicates are referred as Channel 1 and Channel 2.

Samples	As3_0.2	As5_ads	As5_0.8	Rf	χ2	Red-χ2
Exp 1 (FF)- Channel 1	—	—	—	—	—	—
Exp 1 (FF)- Channel 2	17 (2)	23 (7)	65 (6)	0.0038	20.6	0.086
Exp 1 (FF)- Floating film	28 (3)	22 (10)	53 (9)	0.0129	53.8	0.226
Exp 1 (OA)- Channel 1	22 (2)	27 (7)	55 (7)	0.0051	24.5	0.103
Exp 1 (OA)- Channel 2	26 (2)	53 (8)	27 (8)	0.0065	28.8	0.121
Exp 2 (4 mm)- Channel 1	54 (2)	16 (9)	32 (9)	0.0146	36.7	0.158
Exp 2 (4 mm)- Channel 2	49 (2)	22 (7)	32 (6)	0.0076	21.1	0.089
Exp 2 (25 mm)	30 (2)	17 (2)	56 (7)	0.0055	21.9	0.092
Exp 2 (25 mm, Air)	44 (2)	20 (7)	36 (6)	0.0073	20.7	0.087

Table SI-3. Results of the linear combination fitting (LCF) procedure (non-normalized data) applied to Fe K-edge EXAFS of the biogenic precipitate and floating film samples. LCF were performed using the Athena Software on the 2–14 $Å^{-1}$ k-range. The fitted contributions of the Fe species are reported in percentages, without normalizing the sum to 100%. The model compound spectra used in the LCF procedure correspond to the schwertmannite samples "As free", "As3_0.6", and the amorphous ferric arsenate sample "As5_0.8" (Maillot *et al.*, 2013). R-factor (R_f), chi-square (χ^2) and reduced chi-square (Red-χ^2) are given as classical estimators of the goodness of fit. Uncertainties on the contributions are given in parentheses and refer as 3 standard deviation (σ) obtained with the Athena Software. Experimental replicates are referred as Channel 1 and Channel 2.

Samples	As free	As3_0.6	As5_0.8	Rf	χ2	Red-χ2
Exp 1 (FF)- Channel 1	—	—	—	—	—	—
Exp 1 (FF)- Channel 2	28 (8)	34 (10)	31 (5)	0.0084	9.8	0.045
Exp 1 (FF)- Floating film	14 (7)	56 (10)	19 (5)	0.0091	9.2	0.042
Exp 1 (OA)- Channel 1	32 (9)	38 (12)	23 (5)	0.0126	14.5	0.067
Exp 1 (OA)- Channel 2	27 (9)	46 (12)	20 (5)	0.0140	15.8	0.073
Exp 2 (4 mm)- Channel 1	—	—	—	—	—	—
Exp 2 (4 mm)- Channel 2	22 (6)	57 (9)	14 (3)	0.0069	7.5	0.035
Exp 2 (25 mm)	0 (0)	64 (5)	30 (3)	0.0081	9.3	0.042
Exp 2 (25 mm, Air)	19 (6)	56 (9)	18 (3)	0.0072	8.0	0.037

Table SI-4. Micro-X-ray fluorescence data for the biogenic precipitate encrusting the plastic film inserted vertically in the water column of in Exp 2 $_{(4\ mm)\text{-channel } 2}$, Exp 2 $_{(25\ mm)}$ and Exp 2 $_{(25\ mm,\ Air)}$.

	As/Fe molar ratio*		
Height (mm)**	**Exp 2 (4mm) - C2**	**Exp 2 (25 mm)**	**Exp 2 (25 mm, Air)**
0.2	0.76	0.63	0.75
0.7	0.73	0.61	0.74
1.2	0.70	0.61	0.67
1.7	0.68	0.60	0.64
2.2	0.66	0.60	0.63
2.7	0.65	0.59	0.59
3.2	0.64	0.61	0.59
3.7	0.62	0.62	0.58
4.2	0.59	0.68	0.57
4.7	0.59	0.68	0.56
5.2	0.58	0.77	0.55
5.7	0.64	0.62	0.54
6.2	0.64	0.74	0.55
6.7	0.66	0.78	0.54
7.2	0.57	0.80	0.55
7.7	0.59	0.83	0.55
8.2	0.63	0.79	0.56
8.7	0.50	0.78	0.58
9.2	-	0.81	0.61
9.7	-	0.83	0.61
10.2	-	0.87	0.64
10.7	-	0.89	0.65
11.2	-	0.90	0.67
11.7	-	0.93	0.68
12.2	-	0.89	0.68
12.7	-	0.89	0.70
13.2	-	0.91	0.70
13.7	-	0.90	0.70
14.2	-	0.88	0.71
14.7	-	0.80	0.72
15.2	-	0.78	0.73
15.7	-	0.79	0.74
16.2	-	0.76	0.76
16.7	-	0.78	0.78
17.2	-	0.82	0.78
17.7	-	0.87	0.79
18.2	-	0.88	0.81
18.7	-	0.93	0.81
19.2	-	0.96	0.84
19.7	-	0.96	0.86
20.2	-	0.97	0.86
20.7	-	0.88	0.90
21.2	-	0.83	0.91
21.7	-	0.78	0.96
22.2	-	0.76	0.95
22.7	-	0.84	0.91
23.2	-	1.21	0.84
23.7	-	0.78	0.80
24.2	-	1.58	0.84
24.7	-	1.58	0.84
25.2		-	0.86

* As/Fe ratio is calculated by dividing the integrated areas under the Kα peaks of As and Fe, and taking into account As and Fe fluorescence absorption coefficients

**Height is the height of analysis on the plastic films; 0 stands for the bottom of the channel

Table SI-5. Results of the LCF procedure (non-normalized data) applied to micro-XANES. Reduced χ^2 is given as an estimator of the goodness of fit.

	Exp 2 $_{(4\ mm)-\ Channel\ 2}$ - XANES LCF			**Exp 2 $_{(25\ mm)}$ - XANES LCF**			**Exp 2 $_{(25\ mm,\ Air)}$ - XANES LCF**		
Height (mm)*	As(V) ± 3 %	As(III) ± 3 %	Reduced χ^2 ($\times 10^{-2}$)	As(V) ± 3 %	As(III) ± 3 %	Reduced χ^2 ($\times 10^{-2}$)	As(V) ± 3 %	As(III) ± 3 %	Reduced χ^2 ($\times 10^{-2}$)
0.1	45	56	1.46	50	54	1.33	50	53	1.35
1.1	44	57	1.42	44	59	1.48	46	58	1.46
2.1	38	62	1.42	39	64	1.40	41	63	1.36
3.1	34	67	1.29	36	67	1.43	38	66	1.28
4.1	30	71	1.23	35	68	1.18	36	69	1.38
5.1	31	71	1.22	35	68	1.21	34	71	1.31
6.1	36	65	1.27	42	61	1.30	33	72	1.25
7.1	28	73	1.16	56	48	1.19	36	68	1.31
8.1	24	78	1.20	54	49	1.18	41	63	1.47
9.1	37	65	3.68	54	50	1.14	46	57	1.51
10.1	-	-	-	56	47	1.20	49	53	1.39
11.1	19	81	1.60	65	39	1.03	52	51	1.39
12.1	31	70	1.31	68	36	1.09	53	50	1.34
13.1	-	-	-	70	34	1.17	59	43	1.30
14.1	-	-	-	71	33	2.42	59	43	1.39
15.1	-	-	-	71	33	0.99	62	40	1.32
16.1	-	-	-	71	33	9.35	63	38	1.30
17.1	-	-	-	68	36	1.03	66	35	1.30
18.1	-	-	-	69	35	0.94	68	33	1.01
19.1	-	-	-	78	26	0.82	70	31	1.01
20.1	-	-	-	79	25	0.96	70	30	1.41
21.1	-	-	-	82	23	0.89	73	27	1.37
22.1	-	-	-	78	26	0.94	72	28	1.70
23.1	-	-	-	75	29	1.05	60	41	4.11
24.1	-	-	-	82	22	0.90	61	39	3.15

* Height is the height of analysis on the plastic film; 0 stands for the bottom of the channel

6. FIGURES

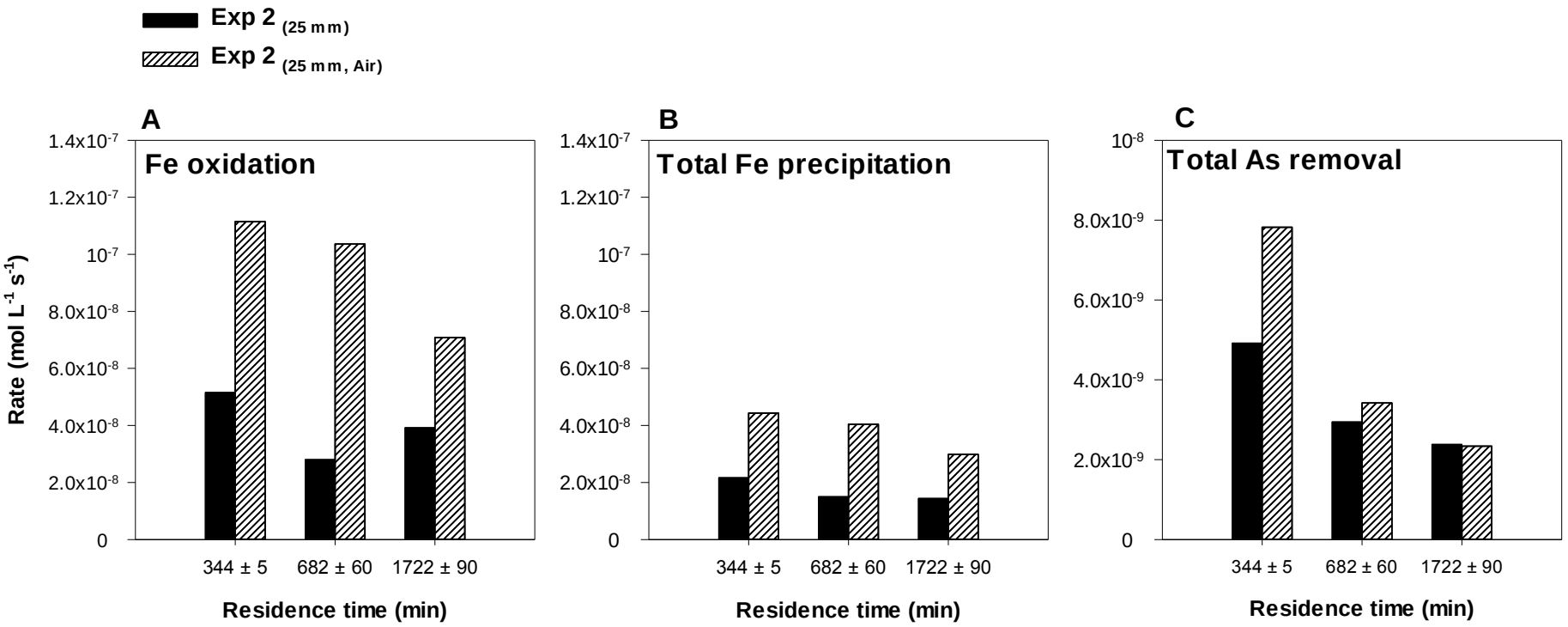

Figure SI-1. Fe oxidation (A), total Fe precipitation (B) and total As removal (C) in Exp 2 $_{(25\ mm)}$ and Exp 2 $_{(25\ mm,\ Air)}$ determined at three different residences times.

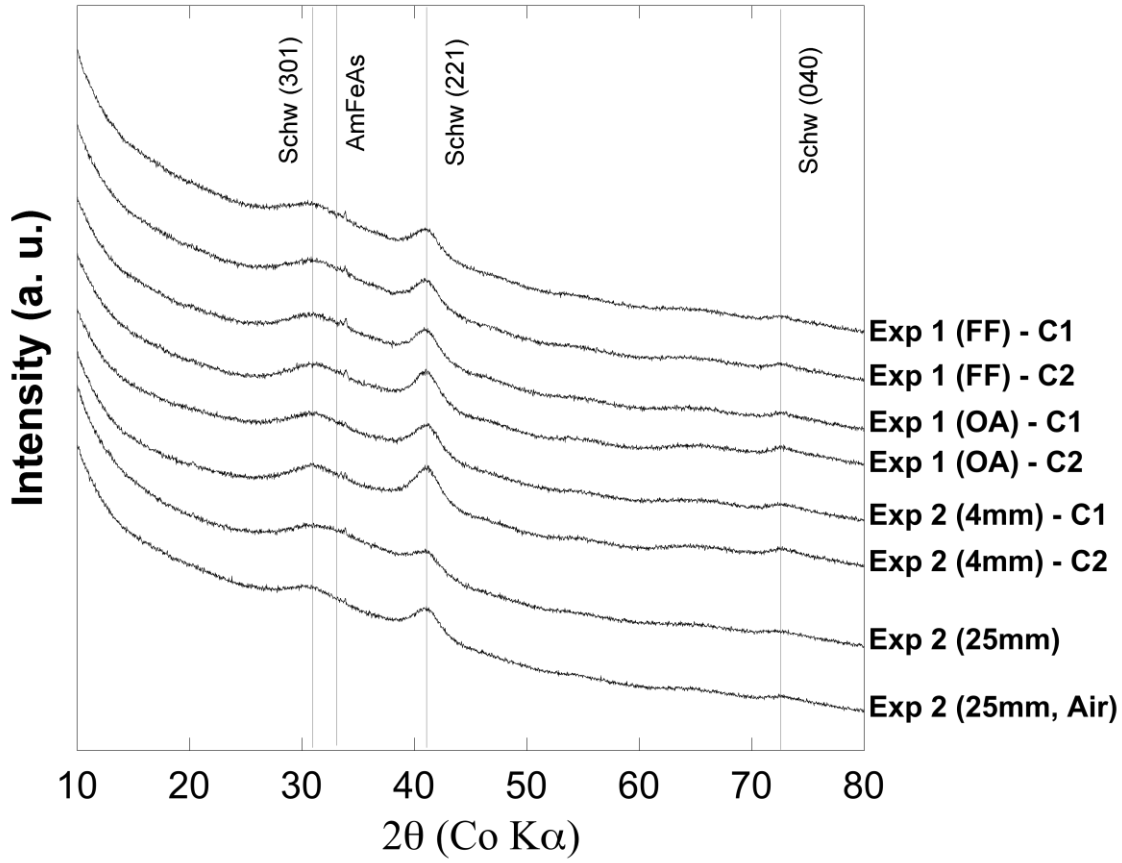

Figure SI-2. Powder X-Ray diffraction patterns of the biogenic precipitates. Experimental replicates are referred as Channel 1 (C1) and Channel 2 (C2)

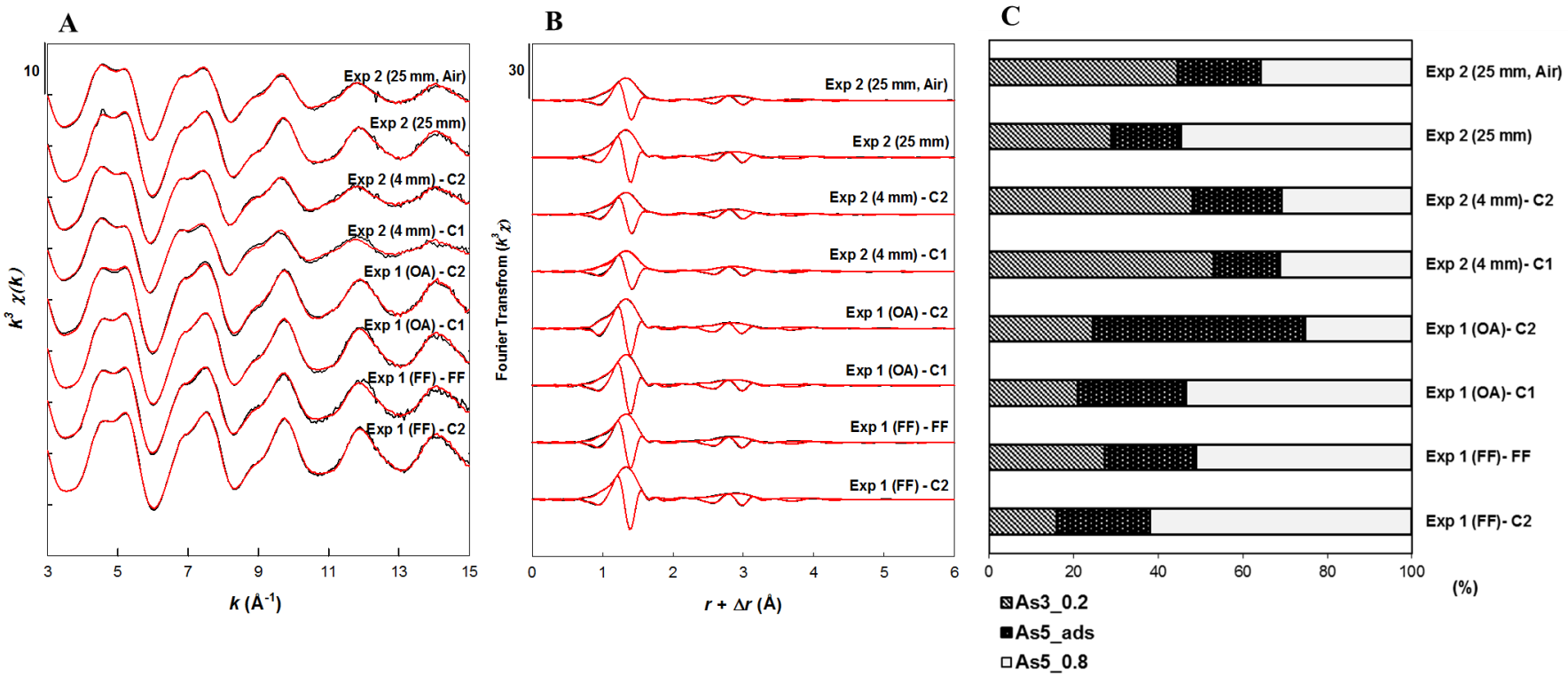

Figure SI-3. LCF of As K-edge EXAFS data of the biogenic precipitate and floating film samples. Experimental and fit curves are displayed in black and red lines, respectively. (A) k^3-weighted EXAFS and (B) their Fast Fourier transforms. (C) Normalized molar proportions of the LCF components in each sample, with respect to total arsenic. The three fitting components, described in detail by Maillot *et al.* (2013), are the following: As(III)-coprecipitated schwertmannite with As/Fe = 0.2 mol/mol (As3_02), As(V)-sorbed schwertmannite with As/Fe = 0.01 mol/mol (As5_ads) and Amorphous Ferric Arsenate with As/Fe = 0.8 mol/mol (As5_0.8). Redox state of arsenic determined from LCF analysis of the XANES region of the same data are given in Resongles *et al.* (2016) (see Table SI-1), and fall within the standard deviation obtained from the present EXAFS LCF results, as given in Table SI-2. Experimental replicates are referred as Channel 1 (C1) and Channel 2 (C2).

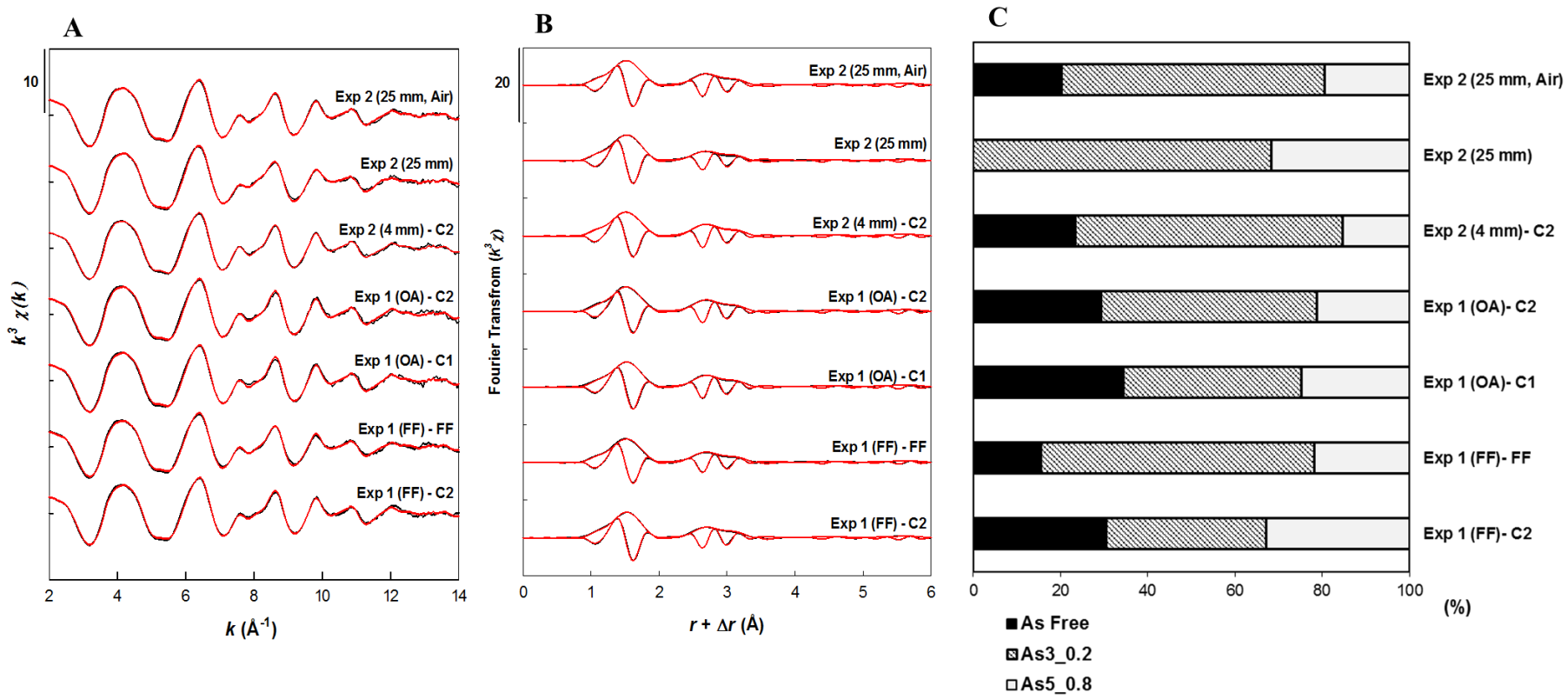

Figure SI-4. LCF of Fe K-edge EXAFS data of the biogenic precipitate and floating film samples. Experimental and fit curves are displayed in black and red lines, respectively. (A) k^3-weighted EXAFS and (B) their Fast Fourier transforms. (C) Normalized molar proportions of the LCF components in each sample, with respect to total iron.The three fitting components, described in detail by Maillot *et al*. (2013), are the following: As-free schwertmannite (As Free), As(III)-coprecipitated schwertmannite with As/Fe = 0.2 mol/mol (As3_02), and Amorphous Ferric Arsenate with As/Fe = 0.8 mol/mol (As5_0.8). Results of the LCF are reported in Table SI-3. Experimental replicates are referred as Channel 1 (C1) and Channel 2 (C2).

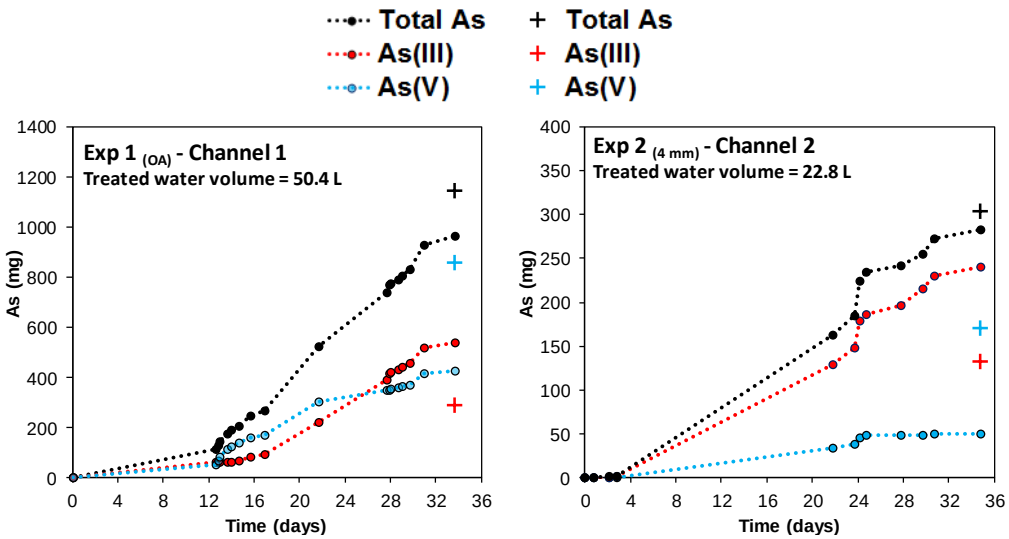

Figure SI-5. Accumulation of arsenic mass (Total As, As(III), As(V)) removed from the dissolved phase as a function of time (dots) in Exp 1 (OA) and Exp 2 (4 mm), and arsenic mass measured in the biogenic precipitate at the end of each experiment (crosses). This figures only includes the treatment replicates whose estimations have an error lower than 16 % between the calculated Total As removed from the dissolved phase and the Total As found in the biogenic precipitate. For the rest of the experiments, calculations did not match the measured arsenic in the biogenic precipitate because of the lack of sampling points (Exp 1 (FF)), or the higher treated water volume (Exp 2 (25 mm)) which does not provide a good extrapolation from few points. The other treatment replicate from Exp 1(OA) and Exp 2 (4 mm) has an error of 19 % and 21 % respectively.

Equations used to calculate the As mass accumulated at time "t_i":

$$As\ load_{t_i} = As_{t_i}\ (mg\ L^{-1}) * Q_{t_i}\ (L\ s^{-1})$$

$$As\ mass_{t_i} = \int_{t_{i-1}}^{t_i} As\ load(t)\ dt = \left[\frac{As\ load_{t_i} + As\ load_{t_{i-1}}}{2}\right] \times (t_i - t_{i-1})$$

$$As\ mass\ accumulated_{t_i} = (As\ mass\ inlet_{t_i} - As\ mass\ outlet_{t_i}) + As\ mass\ accumulated_{\ t_i-1}$$

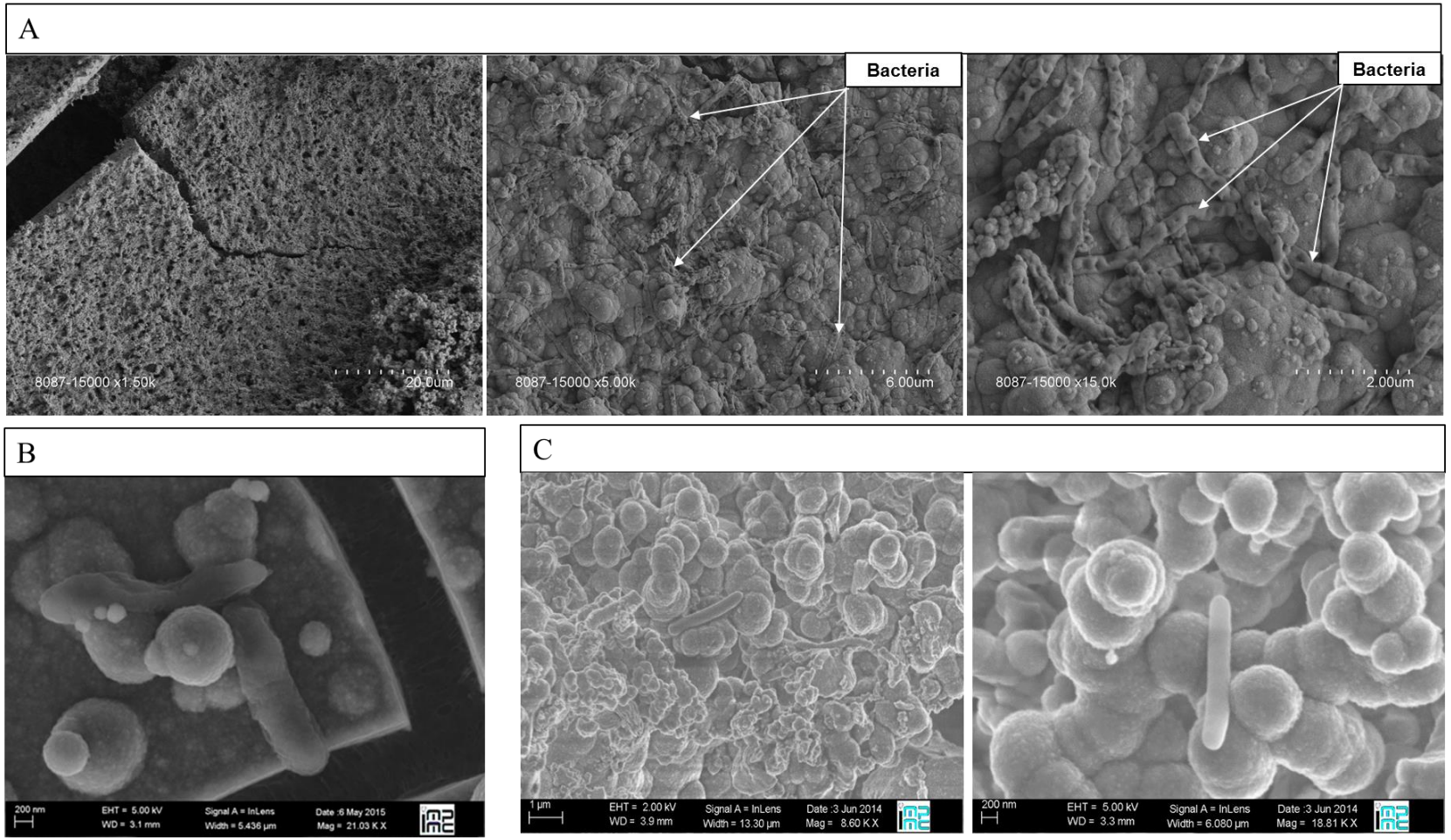

Figure SI-6. SEM images at different scales of (A) the floating film, (B) the precipitates deposited on the plastic films inserted in Exp 2. (C) typical precipitates collected at the bottom of the bioreactor. The mineral spheroids with stitched surface exhibit characteristic morphology of As-rich schwertmannite.

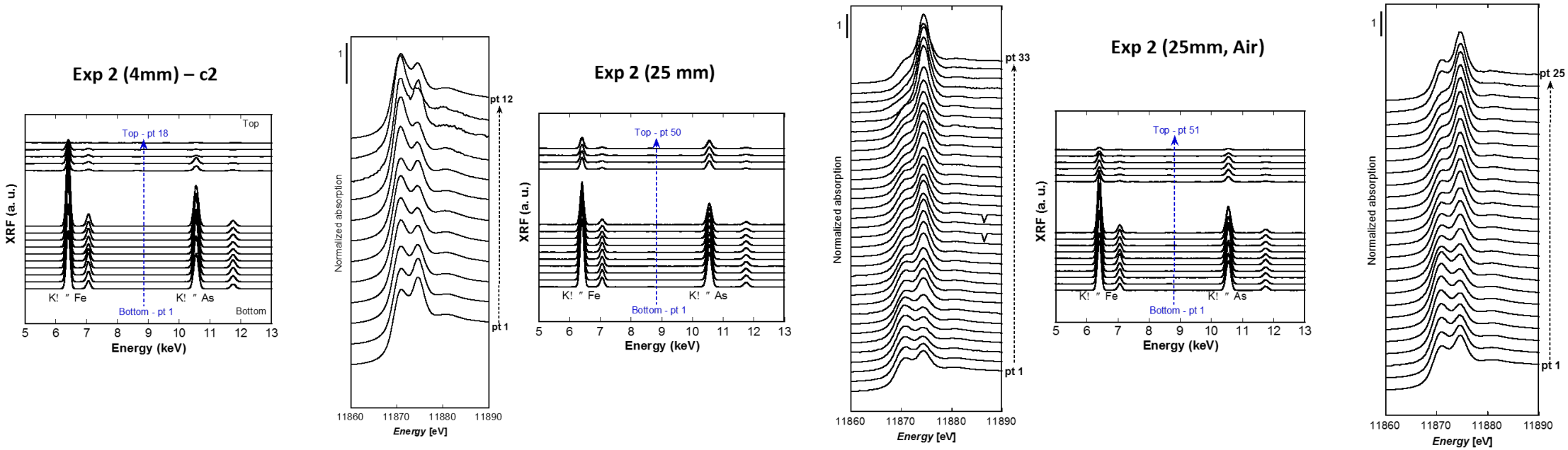

Figure SI-7. Micro XRF bulk spectra and spatially resolved XANES bulk spectra of the results presented in Figure 6. The molar As/Fe and As(III)/As(V) ratio values calculated using those spectra are given in Tables SI-4 and SI-5.

7. REFERENCES

Cardinale, M., Brusetti, L., Quatrini, P., Borin, S., Puglia, A.M., Rizzi, A., Zanardini, E., Sorlini, C., Corselli, C., Daffonchio, D., 2004. Comparison of different primer sets for use in automated ribosomal intergenic spacer analysis of complex bacterial communities. Applied and Environmental Microbiology 70 (10), 6147–6156. doi:10.1128/AEM.70.10.6147-6156.2004

Casiot, C., Morin, G., Juillot, F., Bruneel, O., Personné, J.-C., Leblanc, M., Duquesne, K., Bonnefoy, V., Elbaz-Poulichet, F., 2003. Bacterial immobilization and oxidation of arsenic in acid mine drainage (Carnoulès creek, France). Water Research 37 (12), 2929–2936. doi:http://dx.doi.org/10.1016/S0043-1354(03)00080-0

Héry, M., Casiot, C., Resongles, E., Gallice, Z., Bruneel, O., Desoeuvre, A., Delpoux, S., 2014. Release of arsenite, arsenate and methyl-arsenic species from streambed sediment affected by acid mine drainage: a microcosm study. Environmental Chemistry 11 (5), 514. doi:10.1071/EN13225

López-Gutiérrez, J.C., Henry, S., Hallet, S., Martin-Laurent, F., Catroux, G., Philippo, L., 2004. Quantification of a novel group of nitrate-reducing bacteria in the environment by real-time PCR. Journal of Microbiological Methods 57 (3), 399–407. doi: 10.1016/j.mimet.2004.02.009

Lunau, M., Lemke, A., Walther, K., Martens-Habbena, W., Simon, M., 2005. An improved method for counting bacteria from sediments and turbid environments by epifluorescence microscopy. Environmental Microbiology 7 (7), 961–968. doi:10.1111/j.1462-2920.2005.00767.x

Maillot, F., Morin, G., Juillot, F., Bruneel, O., Casiot, C., Ona-Nguema, G., Wang, Y., Lebrun, S., Aubry, E., Vlaic, G., Brown Jr, G.E., 2013. Structure and reactivity of As(III)- and As(V)-rich schwertmannites and amorphous ferric arsenate sulfate from the Carnoulès acid mine drainage, France: Comparison with biotic and abiotic model compounds and implications for As remediation. Geochimica et Cosmochimica Acta 104, 310–329. doi:http://dx.doi.org/10.1016/j.gca.2012.11.016

Quéméneur, M., 2008. Les processus biogéochimiques impliqués dans la mobilité de l'arsenic: recherche de bioindicateurs. PhD thesis, Nancy University, 21st November 2008.

Quéméneur, M., Cébron, A., Billard, P., Battaglia-Brunet, F., Garrido, F., Leyval, C., Joulian, C., 2010. Population structure and abundance of arsenite-oxidizing bacteria along an arsenic pollution gradient in waters of the Upper Isle River basin, France. Applied Environmental Microbiology 76 (13), 4566-4570.

Ravel B. and Newville M. (2005) ATHENA, ARTEMIS, HEPHAESTUS: data analysis for X-ray absorption spectroscopy using IFEFFIT. Journal of Synchrotron Radiation 12 (4), 537–541.

Resongles, E., Casiot, C., Freydier, R., Dezileau, L., Viers, J., Elbaz-Poulichet, F., 2014. Persisting impact of historical mining activity to metal (Pb, Zn, Cd, Tl, Hg) and

metalloid (As, Sb) enrichment in sediments of the Gardon River, Southern France. Science of the Total Environment 481, 509–521. doi:10.1016/j.scitotenv.2014.02.078

Resongles, E., Le Pape, P., Fernandez-Rojo, L., Morin, G., Brest, J., Guo, S., Casiot, C., 2016. Routine determination of inorganic arsenic speciation in precipitates from acid mine drainage using orthophosphoric acid extraction followed by HPLC-ICP-MS. Analytical Methods 8, 7420–7426. doi:10.1039/c6ay02084d

Rodier, J., Broutin, J., Chambon, P., Champsaur, H., Rodi, L., 1996. L'analyse de l'eau. Paris: Dunod, 1383 p.